Sahar Abdellatif, BSc

Master Thesis 2018 supervised by:

Prof. Holger OTT

Feasibility of Surfactant-Based EOR Mechanisms in Microfluidics

dpe DEPARTMENT PETROLEUM ENGINEERING

MONTAN UNIVERSITÄT

EIDESSTATTLICHE ERKLÄRUNG

Ich erkläre an Eides statt, dass ich diese Arbeit selbständig verfasst, andere als dieangegebenen Quellen und Hilfsmittel nicht benutzt und mich auch sonst keiner unerlaubten Hilfsmittel bedient habe.

AFFIDAVIT

I hereby declare that the content of this work is my own composition and has not been submitted previously for any higher degree. All extracts have been distinguished using quoted references and all information sources have been acknowledged.

Acknowledgements

I am grateful to the God for the good health and wellbeing that were necessary to complete this book.

I am also grateful to Prof. Holger OTT, in the Department of the reservoir. I am extremely thankful and indebted to him for sharing expertise, and sincere and valuable guidance and encouragement extended to me.

I take this opportunity to express gratitude to all my family members and friends for their help and support. I also thank my mother Hajer Abdellatif for the unceasing encouragement, support, and attention.

I dedicate this work to my dear father's soul Kamel Abdellatif, who was the drive for my success and he was always there for me. I hope that your soul rests in peace

Abstract

The Oil and Gas industry is since decades aware that the time of “easy oil” is ending. Most of the world's largest producing fields are nearing depletion, and most of the remaining reserves are considered challenging to recover. This fact motivates the industry to develop and implement innovative EOR techniques to enhance the oil recovery. In fact, EOR techniques aim to modify reservoir parameters either by increasing the mobility ratio (Eq. 13) or by improving the capillary number (Eq. 5).

The first goal of the thesis is to examine the effect of decreasing IFT and mobility ratio by flooding different solutions for oil displacement in glass microfluidic devices (micromodels) in order to investigate pore-level displacement mechanisms for EOR.

The experiments have been performed using surfactant, polymer and surfactant-polymer flooding; aqueous solutions with different concentrations were injected into microchips saturated with oil from Matzen field (16TH reservoir). The injection experiments were performed in secondary and tertiary recovery modes.

The results observed from the tests showed that both surfactant flooding and surfactant-polymer flooding yield to the highest recovery factor due to their ability to reduce IFT, the place by enhancing the mobility ratio, while the pure water flooding had the lowest recovery factor.

Furthermore, the addition of surfactant to the injection water may lead to foam generation. Another focus of thesis was to study foam generation mechanisms and to analyse foam quality by investigating the bubble sizes and by the quantification of the characteristic times for the evolution of the foam. In addition, an investigation was carried out to examine the relationship between the bubble sizes and bubble mobility. The experiment result showed that the small bubbles have higher velocity compared to the larger ones,

Table of Contents

List of Figures

List of Equations

List of Tables

Nomenclature

Absolute permeability	$Kabs$	[Darcy]
Average (Darcy) velocity	uD	[cm/s], [m/s]
Capillary pressure	Pc	[Pa]
Cluster length	lcl	[m]
Cross sectional area	A	[cm2]
Differential pressure	ΔP	[bar]
Flow rate	q	[cm3/s]
Injection flow rate	qinj	[mm3/h]
Interfacial tension	σ	[dyne/cm]
Interstitial velocity	v	[m/s]
Length	L	[cm]
Macroscopic capillary number	$NCmacro$	[-]
Microscopic capillary number	$NCmicro$	[-]
Pressure gradient	∇P	[bar/cm]
Pusher block velocity	vpb	[mm/h]
Relative permeability to wetting phase	Krw	[-]
Syringe inner diameter	$dsng$	[mm]
Viscosity	μ	[cp], [Pa. s]

Abbreviations

Areal Sweep Efficiency	EA
Capillary Desaturation Curve	CDC
Critical Micelle Concentration	CMC
Differential Pressure Transmitter	DPT
Enhanced Oil Recovery	EOR
Hydrocarbon	HC
Interfacial Tension	IFT
Reactive Ion Etching	RIE
Representative Elementary Area	REA
Torton Horizon	TH
Total Acid Number	TAN
Unit Displacement Efficiency	ED
Volumetric Sweep Efficiency	EV
Water in Oil	W/O
Alkane Carbon Number	ACN

1 Fundamentals of EOR

This chapter presents a summary of the basic fundamentals of different oil recovery stages; primary, secondary, tertiary and their limitations and disadvantages.

The standard mechanism of oil recovery is the hydrocarbons migration caused by the pressure difference between the production wells and the reservoir. The improvement of oil reserves is split into three broad categories. Figure 1 shows these types:

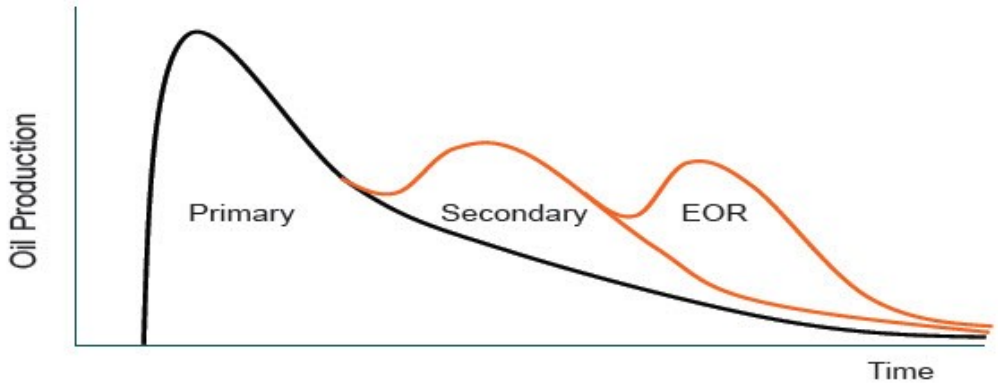

Figure 1: Recovery stages of a hydrocarbon over the reservoir lifetime

Primary recovery procedures: “This technique takes place in the initial production stage, which results from the displacement force naturally existing in a reservoir” [1]

Secondary recovery procedures: “Commonly used when the primary production starts to decline. Usually these methods are based on pressure maintenance by, water flooding, and gas injection, or are based on viscous displacement of oil by the injection water. The recovery factor can increase to 50%.” [1]

Tertiary recovery procedures: “These techniques are related to the methods applied in the secondary recovery technique. Normally, these methods use thermal energy and/or miscible gases, chemicals to further displace oil after the secondary recovery techniques have become uneconomical. The recovery factor may rise further 12% in addition to that achieved with the secondary recovery techniques.” [1]

1.1 Recovery Stages

As stated before, the hydrocarbons are produced by various methods and techniques. The application of oil recovery methods depends upon factors such as:

- Volumetric displacement efficiency: It is a visible displacement effect on a function of mobility ratio (*M*). The water flooding effectiveness can be enhanced by decreasing the water-oil mobility rate. Fluid mobility (λ = permeability/fluid viscosity) is a quantitative measure of its capacity to flow via the channels

$$\mathbf{M} = \left(\frac{\mathbf{Krw}}{\mu\mathbf{w}}\right) \Big/ \left(\frac{\mathbf{Kro}}{\mu\mathbf{o}}\right) \quad [2] \qquad (1)$$

Where: K_{rw} = relative water permeability (mD)

K_{ro} = relative oil permeability (mD)

μ_w & μ_o = viscosities of water and oil respectively (cp)

A mobility ratio higher than one is unfavorable because of high water mobility. Water would finger into the oil zone and, consequently, decrease the oil recovery efficiency. If mobility ratio is smaller than one, the oil displacement by water happens in a similar way to piston displacement.

- The displacement efficiency: The fraction of oil that has been produced from a zone swept by a water flood or other displacement method.

$$\mathrm{ED} = \frac{\text{Amount of oil displaced}}{\text{Amount of oil contacted by displacing agent}} [3] \qquad (1)$$

Rock, fluid and rock-fluid properties also influence ED. If the displacing fluid contacts all the initial oil existing in the reservoir, the volumetric sweep efficiency will be one.

- Volumetric Sweep Efficiency:

$$\mathrm{EV} = \frac{\text{Volume of oil contacted by dispacing fluid}}{\text{Total amount of oil in place}} [4] \qquad (2)$$

- EV can be split into two components, vertical areal sweep efficiency.

$$\mathbf{EV} = \mathbf{EA} * \mathbf{ET}\ \mathbf{[4]} \qquad (3)$$

$$\mathrm{EA} = \frac{\text{Area contacted by displacing fuid}}{\text{Total area}} \qquad \mathrm{ET} = \frac{\text{Cross-sectional area contacted by displacing fluid}}{\text{Total cross-sectional area}}$$

The following part will explain the recovery stages exhibited during the lifetime of the reservoir.

1.1.1 Primary Recovery

In this recovery method, oil is carried out via the natural trapped fluids pressure already existed in the reservoir. In primary oil recovery process, the efficiency of oil displacement depends principally on the natural pressure exists in the reservoir. Some reasons for this pressure in the reservoir are:

- Expanding force of natural gas
- Buoyancy force of invading water
- Gravitational force
- An expulsion force caused by the compaction of unconsolidated reservoir rocks [1]

Amongst these forces, the increasing of the natural gas pressure contributes essentially to oil production. In the reservoir, these forces either can work sequentially or simultaneously, depend on the reservoir features and composition. The gravitational force is strongly effective in steeply inclined reservoirs, where the oil drainage becomes much easier. The gravitational force individually may not be useful in removing massive oil quantities into a production well. The water invasion from the side or bottom of the reservoir is another force for oil displacement. The edge water capacity to encroach based on the permeability and pressure pattern. The reservoir compaction as fluids are removed is also a procedure for the discharge of oil to production wells. Due to the reduction in the reservoir volume, part of the oil will be removed.

1.1.2 Secondary Recovery

At the time when the reservoir pressure decreases, and the primary mechanism are no more used as a mechanism of hydrocarbons flow to the wells, gas or water is injected to increase the reservoir pressure. Some wells are converted to injection wells to keep the pressure in the reservoir:

- Pressure restoration
- Pressure sustaining

The secondary oil recovery mechanism is comparable to the primary oil recovery with one more wellbore is required, and the reservoir pressure is increased or sustained to push oil into the production wells. The method involves the utilization of gas or water injection.

1.1.3 Restrictions and drawbacks of Primary and Secondary Recovery Methods

The fast drop in reservoir pressure drives to moderate oil production rates and oil recovery (5 – 10 % of OIP [1]). Secondary recovery (gas/water injection) usually doesn't produce a large recovery because of:

- The heterogeneity of the reservoir
- Unfavorable mobility ratio between water and oil
- Gas and water coning issues
- Moderate sweep efficiency

It is an important thing to know when it is the right time to start applying EOR mechanisms and determine when and under which condition to be used. The determination of the optimum time for applying EOR methods is based on:

- Predicted oil recovery
- Fluid production rates
- Financial investment
- Pumping cost equipment and water treatment
- Operation and maintenance cost of the water installation equipment
- Drilling cost further injection wells or changing the production wells (already exist) into injectors

1.1.4 Enhanced Oil Recovery Methods (EOR)

Enhanced oil recovery applies to reservoir, which are depleted by means by conventional primary and secondary production methods, resulting in a low declining production rate. EOR is designated to increase the displacement and sweep efficiency by injecting fluids injections to decrease the residual oil saturation beneath the level reached by conventional techniques. The oil in areas not flooded by the injected fluid and the oil trapped in the swept areas by capillary forces which are involved in remaining oil description. Examples are surfactant flooding for reducing capillary trapping and polymer flooding stabilizing the flood front and increasing therefore the sweep.

In brief, the EOR objective is recovering a significant amount of the remaining OIP by modifying rock and fluid properties. EOR processes can be categorized as:

- Chemical methods
- Thermal methods
- Miscible displacement methods

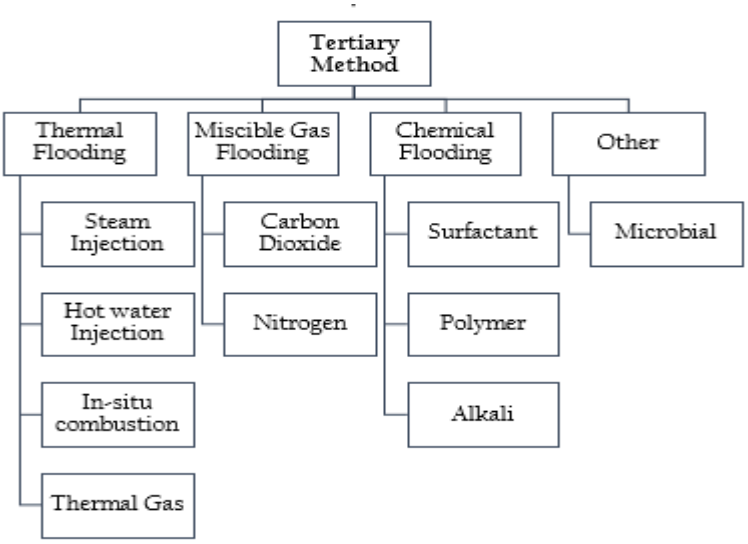

Figure 2: Classification of the different EOR methods

1.1.5 Chemical processes

The main concept of chemical flooding is adding chemical to the injection water in order to modify chemical and physical rock and fluid properties in order to improve displacement. Chemical flooding methods can be grouped into three classes:

- Surfactant flooding
- Polymer flooding
- Alkaline (caustic) flooding

In chemical flooding, the different solutions can be injected individually and subsequently or mixtures in one slug; a good example is Alkaline-Surfactant-Polymer Flooding (ASP) where both methods are applied in practice. In the reservoir, the injected alkaline acts chemically with the fatty acids of the oil phase forming in-situ surfactant. The surfactant decreases the interfacial tension with the side effect of wettability alteration, while polymer is applied to enhance the invading fluid sweep efficiency by altering the mobility ratio. The formation of

these surfactants causes a low IFT. The chemical flooding methods have been schematically demonstrated in Figure 2 above.

2 Chemical EOR

One of the EOR techniques is chemical flooding, which includes the alkalis, polymer, surfactant and their combinations to increase oil recovery. In other words, the primary aims of oil recovery in chemical flooding is decreasing of capillary forces.

In the porous media, the non-wetting phase (e.g. oil) mobilization can be prophesied by the balance of capillary forces and viscous forces, which is called capillary number. One of the most direct and generally used definition of capillary number related to microscopic capillary number is as follows:

$$N_{micro}^{C} = \frac{\nu\,\mu}{\sigma} \qquad (1)$$

Where N_{micro}^{C} is the microscopic capillary number, ν is the interstitial velocity, μ is the viscosity of displacing fluid, and σ is the IFT.

Residual oil saturation relationship with capillary number had been investigated by experiments and research. So capillary "desaturation "curves "(CDCs) [2] was created as presented in Figure 3:

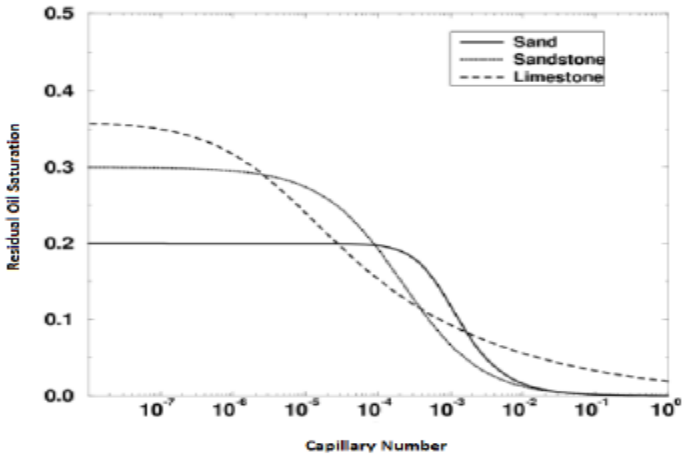

Figure 3: Schematic capillary desaturation curves for limestone, sand, and sandstone.

Additional experimental data determined that the residual trapped non-wetting phase mobilization happens at N_{micro}^{C} between 10^{-5} and 10^{-7}. However, these results are limited to the specific rock type and hence, are non-predictive. Furthermore, mobilization is expected to occur at ratio of the capillary to viscous forces of one. The discrepancy appears from the N_{micro}^{C} definition in equation (5), which is the interfacial definition that balance the interfacial stress to the viscous stress at the same interface [2]. In other terms, the definition of N_{micro}^{C} pretends

that capillary and viscous forces behave over the similar length scale and deletes the shape of the trapped non-wetting phase topology Melrose and Brandner (1974) [3]. For the first time, a model was established to account for the non-wetting phase and pore-space topology, so the term macroscopic capillary number was proposed. Hilfer and Øren (1996) [5] were made a modification after a detailed scaling analysis by connecting the microscopic and macroscopic pictures. Nonetheless, non-wetting phase desaturation was witnessed at the macroscopic capillary number underneath one [3]. A macro-scale capillary number was provided and presented by Hilfer and Øren [5] by incorporating relative permeability into the equation as follows:

$$\mathrm{N}^{\mathrm{C}}_{\mathrm{macro}} = \frac{\mathrm{lcl}\,\mu\,\nu}{\mathrm{k_{rw}Pc}}\,[5] \qquad (2)$$

Where N^{C}_{macro} is the capillary number, μ is the viscosity of displacing fluid, lcl is the cluster length, v is the Darcy velocity , k_{rw} is the relative permeability to displacing fluid, and P_C is the capillary pressure.

2.1 Surfactant Methods

2.1.1 Introduction

It is well known in oil and gas industry , that the capillary force is the cause of massive quantities of oil left behind in good-swept zones of water flooded oil reservoirs. For a more significant amount of residual oil production, surfactants should be injected. This section will present an overview of this technology.

The primary function of the surfactants are decreasing the interfacial tension and altering the wettability. The use of surfactant flooding depends on these two features.

2.1.2 Wettability alteration

The carbonates are known for being likely oil wet. Furthermore, they were the target of wettability alteration mechanism. The water imbibition is improved, as the rock becomes more water-wet , and the remaining oil saturation is reduced. The effect of the surfactant is visible especially in naturally fractured carbonate reservoirs, where, the matrix changes to more water-wet. The water imbibition displaces the oil through the matrix blocks. Some researchers proposed that the relative permeability and capillary pressure figures resulting from wettability alteration [4].The research was done by Sheng, where he compared a various methods effects of oil recovery associated with surfactants injection. Especially, the IFT reduction and wettability alteration were analyzed. Using the numerical simulation method ,

the wettability has a significant role, when the IFT is high, and it is active at the early time. Hence, the IFT effect does not rely on the wettability alteration, where it is efficient with or without it during the process.

2.1.3 Interfacial Tension Reduction

To demonstrate the interfacial tension function, first, it is important to understand the relationship between capillary numbers and residual oil saturation that been described in the previous section

Several experiments results prove that the residual saturations are increasing when the capillary number is decreasing. The relationship between the capillary number and residual saturation is described by the capillary desaturation curve as explained before.

Based on the capillary number definition Eq. (5), there are three principals ways; the first one is increasing displacing fluid viscosity μ, the second method is raising the injection fluid velocity u, the last one which is more applicable in filed is a reduction of the IFT. It is evident that the capillary number can't be increased 1000 times by the first two modes.

Several tests prove that the IFT between oil and surfactant can be decreased from in the order of 10^{-3} mN/m, so by using the surfactant, the capillary number can be improved by more than 1000 times. Lower the IFT cause the capillary number to decrease which let the oil droplets move more smoothly through pore throats. The oil droplets flow ahead and mix with the oil to create an oil bank. A different method is associated with swelling. In the type I micro-emulsion, oil drops are solubilized in the water phase. In the type II micro-emulsion, water drops are solubilized in the remaining oil. As a result, the oil quantity becomes more important. In type III micro-emulsion, both oil and water solubilize in each other creating an intermediate phase. Solubilisation causes the oil to swell; the oil phase saturation becomes higher, because of increase in the oil relative permeability. Therefore, it is much smoother for the oil to flow. The residual saturation reduction is due to the surfactant injection which causes an improvement in the relative permeability. In large aqueous phase saturation range, the aqueous phase to oleic phase permeability ratio is decreased. So, the surfactant injection improves the oil sweep efficiency.

- **The effect of Different Factors on Interfacial Tension**

In the previous section, the main surfactant mechanism which is the decreasing of IFT was discussed, which is closely associated with oil and water solubilisation.

The next section will explain the factors that affect the IFT in more details. IFT is affected by several parameters, such as the surfactant type and its concentration. the divalent, salinity and oil composition (ACN: alkane carbon number), solvent and its concentration , water-oil ratio, and the system parameters (pressure and temperature).Surfactant concentration is one of some parameters that are ambitious to guess their effects qualitatively; it is more probable that a higher surfactant concentration caused a lower IFT, and for another, the increasing of

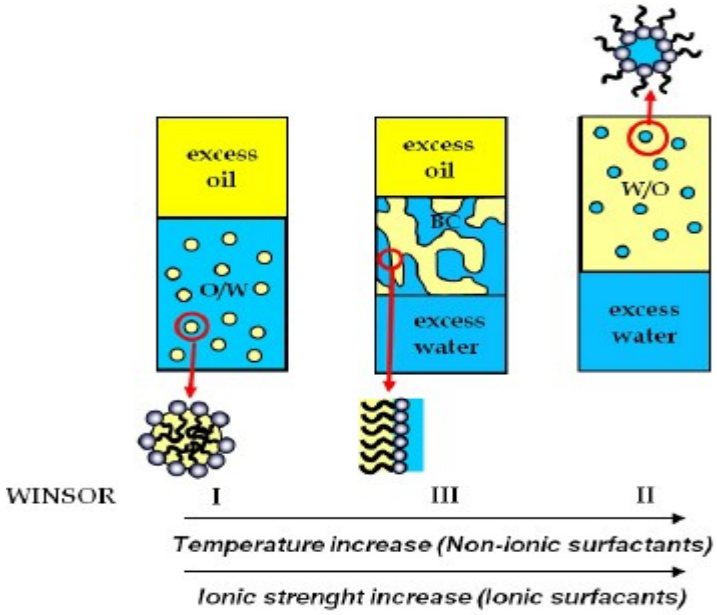

Figure 4: Scheme of the oil/ water microemulsions types

surfactant concentration will the increase the IFT. The optimum salinity is one relevant parameter. A system with only sodium as composition, the optimum salinity usually doesn't depend on WOR and the surfactant concentration. In a complicated system, the optimum salinity may be based on surfactant concentration. In the case of adding alcohol, the optimum salinity is influenced by WOR.

2.1.4 Trapping Number

The Darcy equation was used and the cos θ is dropped, the capillary number developed into:

$$Nc = \frac{-k\Delta\Phi p/\Delta L}{\sigma} = \frac{k|\vec{\nabla}\Phi p|}{\sigma} \quad [8] \tag{7}$$

Where Φp is the potential of displacing fluid, and ΔΦp /ΔL is the potential gradient , the Bond number is described as:

$$\mathrm{Nb} = \frac{\mathrm{kg}(\Delta\rho)}{\sigma} \quad [8] \tag{8}$$

Where Δρ is the density difference between the displaced fluid and the displacing fluid.

For a one-dimensional, [8] the trapping number is:

$$\mathrm{Nt} = \mathrm{Nc} + \mathrm{Nb}\sin\alpha \tag{9}$$

For a two-dimensional flow , the trapping number is described by the equation below [8]:

$$\mathrm{N_T} = \sqrt{\mathrm{N_C^2} + 2\mathrm{N_C}\mathrm{N_B}\sin(\alpha+\gamma) + \mathrm{N_B^2}} \tag{10}$$

Here γ is the angle between the actual flow direction and the dipping reservoir with the dip angle α (count-clockwise). γ can be estimated from the following relationship [8]:

$$\boldsymbol{\tan(\alpha+\gamma) = \frac{\frac{\partial\Phi p+\Delta\rho g}{\partial t}}{\frac{\partial\Phi p}{\partial t}}} \quad [8] \tag{11}$$

2.1.5 Technical Scanning Number

Several parameters can influence the surfactant flooding; however, the common significant ones are; oil composition, reservoir temperature, clay content divalent contents and formation water salinity. Formation permeability and oil viscosity may have the less significant effects. The Table 1 below shows the surfactant flooding technical screening criteria. Criteria are practical; depend on technical knowledge and field project data about surfactant flooding.

k (mD)	T_f (°C)	Formation water salinity, (TDS, ppm)	Divalent (ppm)	Lithology	Clay	μ_o (cP)	S_o (frac.)	Aquifer	Gas cap	API gravity	Depth, ft
≥20	≤121.1	≤200,000				≤30	≥0.2			≥25	
>20	<93.3	50,000	1000	Sandstone	Low	<20	>0.25	None to week	None to week	>25	NC
>50	<80	Low	Low	Sandstone			>0.3	Weak	Week		<6561
>40	<93.3	<100,000		Sandstone & carbonate		<40					
>20	<93.3	100,000		Sandstone preferred		100	0.3			>25	<9000
>10	<93.3			Sandstone preferred		<35	>0.35			>20	<9000
>50	<70	50,000	1000	Sandstone	Low	<150	0.35	None	None		
>100	<93.3	<200,000 if T_f < 60 °C, <50,000 if T_f > 60 °C,				<35	>0.45			>20	500–9000
152	25.3	39,078		Majority sandstone	Low	5.8	0.4	Generally none	Generally none	36.5	1808
>10	<93.3	<50,000	<100	Sandstone	Low	<35	>0.3	Weak	Weak	NC	NC

Table 1: Review of Surfactant flooding screening criteria

Where it classifies the average values of the relevant factors gathered during surfactant flooding application using the rank and percentile method, the values of the different parameters are examined and being taken at the 50th percentile. Some critical parameters are presented in the next part.

2.1.5.1 Formation, Formation Water Salinity and Divalent

Generally, the surfactants are not used in the carbonate reservoirs compared with the sandstone reservoirs. The reason for this is that the carbonate reservoirs adsorb the anionic surfactants very fast and the use of other surfactant types such as cationic surfactants can be very expensive. For a surfactant EOR application, the clays contents must be small because it causes high surfactant adsorption. Technical screening criteria present formation water salinity and divalent guide. In the field, the reservoir has been under water flooding for some years this is why the reservoir water salinity and the injected water have similar salinity. To achieve the lowest IFT between water and oil, the salinity of injected water should be close to the optimum one. In general, the optimum salinity depends on the composition of crude oil, surfactants type, and its concentration. For different surfactant types, the optimum salinity value isn't high. Sometimes, the surfactant performance can retreat, when it is correlated with divalent.

- **Salinity gradient**

The negative salinity gradient was believed to apply to surfactant flooding. The adverse salinity means that the salinities of pre-flush water slug, surfactant slug, and post-flush slug are in declining order. The negative salinity gradient was introduced based on the relationship that as the surfactant concentration is lowered, the optimum salinity also reduces. The surfactant concentration is reduced as the solution flows forwards due to its adsorption and retention. The optimum salinity decreases as the surfactant flow forwards, that means the optimum

salinity reduces with surfactant concentration. Hence, the reduction of salinity will be consonant with the reduction of optimum salinity, then as the surfactant solution move forwards the optimum salinity is maintained. But in some research, results show that few surfactants have an optimum salinity while the surfactant solution is diluted, so means that the optimum surfactant salinity could rise as the solution flows. If the same logic was followed, a reverse salinity gradient is required. Simulation outcomes present that positive salinity gradient doesn't necessarily drive to larger oil recovery. Hence, this approach is debatable. [5]

2.1.5.2 Viscosity, Oil composition and API gravity

The salinity range is affected by the oil composition within which the IFT is low. Thus, oil composition is significant to surfactant flooring. The examined field application had median oil viscosities of 5.8 cp (see Table 1). A new criterion can't be proved without a special research. Some research incorporates API gravity as a screening factor, but during surfactant flooding, API gravity is more relevant than the effect of viscosity.

2.1.5.3 Aquifer and Gas Cap

In the surfactant flooding, the pressure maintenance is a significant factor. If there is a gas cap or active aquifer, less pressure support is demanded. Therefore, a gas cap or strong aquifer will cause less favorable surfactant flooding.

2.2 Polymer Flooding

Mixing a small amount of polymers with water create a very viscous aqueous fluid. This viscous fluid can decrease mobility ratios in flooding operations significantly. It was recognized as one of the most successful EOR methods. In the 80s, the polymer flooding projects did not improve the reservoir volumetric sweep efficiency. After polymer flooding, the remaining oil saturation is the like water flooding. Nonetheless, the interaction between the polymer solution and the rock surface was observed. This interaction leads to changes in the wettability from oil wet to water wet, which increase the residual oil recovery. Regardless of its ability in changing the wettability, the polymer flooding still cannot produce significant amounts of remaining oil. Polymer flooding doesn't decrease the remaining oil saturation noticeably but is instead a way of reaching the remaining oil saturation more quickly and allows it to be obtained more economically. Therefore, almost the same physical laws used for water floods can be utilized for the polymer solution injection. To perform the oil recovery method with polymer solution more efficient, there are three potential ways:

- By lowering the water-oil mobility ratio.
- Via polymer effects on the fraction flow.

- By redirecting water injection from swept zones.

The oil viscosity and water relative permeability relationship are the principal parameters affecting the reservoir approaching success. These two factors are merged and used in the fractional flow formulation. Pretending that the water and oil are flowing together through a section of a porous media, the fractional flow crude oil, f_o, and water, f_w, can be represented as in Eq.12 [2]:

$$f_o = {}^{1}\Big/_{1+\frac{\mu_o k_{rw}}{\mu_w k_{ro}}} \quad , \quad f_w = {}^{1}\Big/_{1+\frac{\mu_w k_{ro}}{\mu_o k_{rw}}} \tag{12}$$

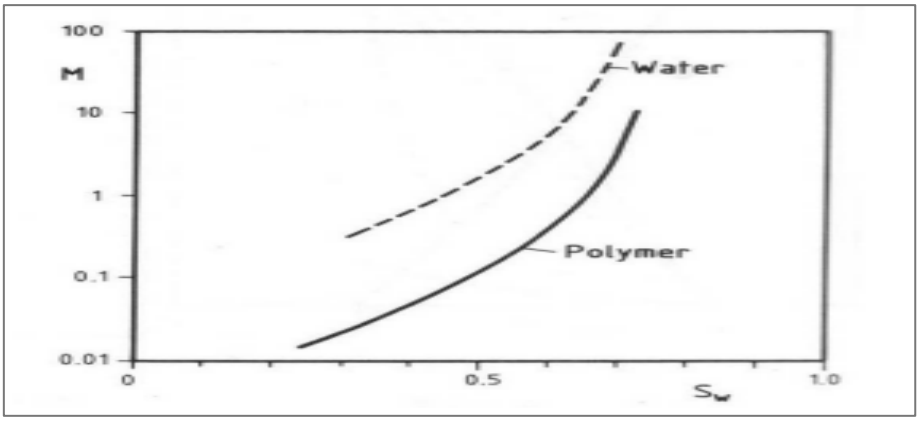

Figure 5: The oil displacement by polymer and water solution as a function of the displacing phase saturation.

Any modification of the term, which raises the oil fractional flow, will lead to an enhancement of recovery. Polymers, when combined with water, can improve the water viscosity, μw. Another impact is that when they have flooded a zone, they can decrease the water permeability k_{rw}. This effect happens at parts of the reservoir having high mobile oil saturation, anyplace where the oil relative permeability is above zero. The changes in water viscosity and water relative permeability will not result in any noticeable improvement in the fractional flow of oil, even with having low mobile oil saturation. Therefore, the fractional flow effect is more meaningful to projects.

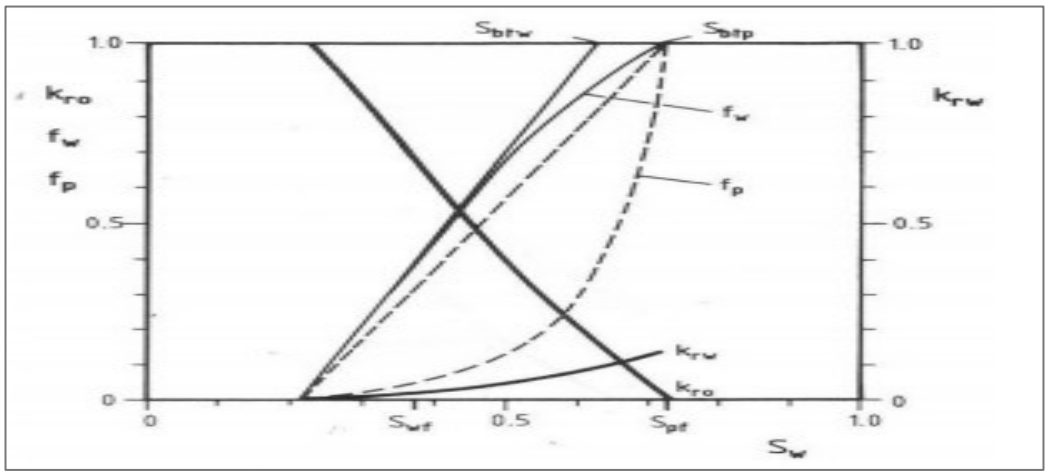

Figure 6: The typical oil and water relative permeability for water-wet sandstone

Where polymer flooding has been implemented early in a field life when moveable oil saturation is still high. Oil viscosities also contribute to the fractional flow. Areas of higher oil viscosity will show the greater tendency of water flowing than oil. Consequently, the water breakthrough and since the water production will be early in the field life and a lot of mobile bypassed oil will be dropped in the reservoir. Therefore, fractional flow effects explain more likely in viscous oil reservoirs. The characteristic flow curves are plotted for oil (15 cp) and the displacing fluids water (1cp) and a polymer solution (15 cp). The different saturations of water Swf, polymer flooding Spf and the saturation at the breakthrough Sbtp are shown in Figure 6. Both the front and the breakthrough saturations are clearly lower for the water flood than for the polymer flood. This tells the better achievement of a polymer flood compared to water flood. The mobility ratios can be below one at low water saturation while the mobility ratio can exceed one for polymer floods at high saturation. The mobility ratio of a flood is defined in Eq.13 as:

$$M = \frac{k_{rw}\ \mu_o}{k_{ro}\ \mu_w} \qquad (13)$$

No real reservoir can be swept consistently, and even in a homogeneous reservoir at water breakthrough a 100 % areal sweep efficiency and an economically water-oil ratio cannot be obtained. For any given reservoir, the recovery till breakthrough will decline with increasing mobility ratio. Also, the later recovery will be less for a given volume of water injected. The polymer solution may increase the mobility ratio in the same way as mentioned above. They can improve the water viscosity or decrease the relative water permeability. It must be considered that at low mobile oil saturation there is only small potential for improvement. From this point of view, a secondary flooding is favorable over a tertiary application for a polymer flooding. Another example of the mobility ratios effect is given in Figure 7. This figure demonstrates the recovery improvement related to a decreasing mobility ratio.

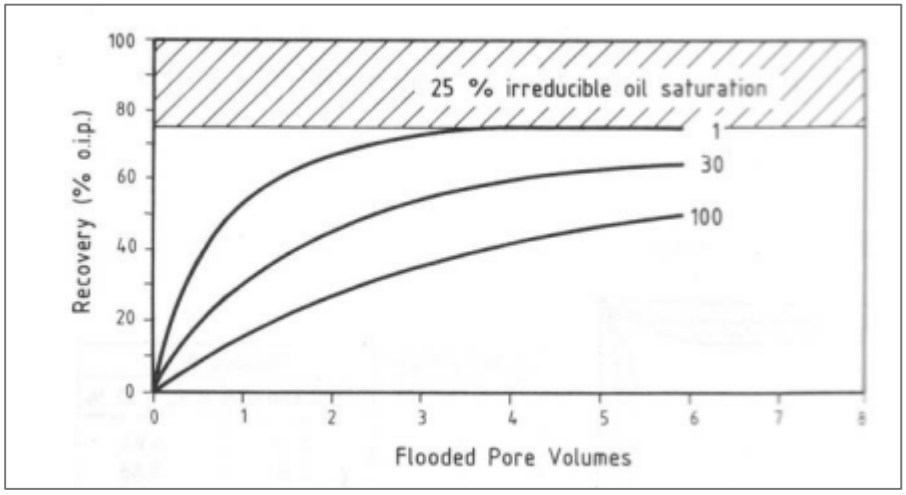

Figure 7: Influence of mobility ratio on oil recovery process.

So far two profitable polymer flooding effects have been shown:

- Faster oil displacement via an improved fractional flow property.
- Areal sweep efficiency enhancement via the improved mobility ratio.

Both these effects essentially work in homogeneous reservoirs and on mobile oil saturation on polymer flooded zones. Unfortunately, no uniform homogenous reservoir exists. The reservoirs majority have important heterogeneities in the areal and especially in the vertical direction. Consequently, water preferentially flows and enters the high permeable zones and sweeps out those areas more rapidly. Ttherefore, the areas which are reached by the flood water are swept efficiently. While, the areas with high flow resistance and low permeability in which water does not flow, stay untouched and have a very low recovery. The injection of the polymer solution into the swept area could recover a small amount of oil out of this zone. However, such polymer solution floods can get very useful because of the fluid diversion. A flow resistance will be created by polymer through permeability decrease in the penetrated parts of the reservoir. The polymer floods started at high water-oil ratios, resulted in higher the recovery compared to fractional flow. During the flooding, the good results are achieved when the polymers physical properties can be sustained over an extended the lifetime of the project. This leads to set a premium on permeability decrease against the viscosity enhancement because the reduction of permeability can be long-lasting. Optimized permeability modification makes cross-linking of the polymer wanted. The fluid diversion was the most important effect at high water-oil ratios condition. Because of the low oil relative permeability values in the swept zones, the fluid diversion helps in increasing the recoveries in the poor swept areas.

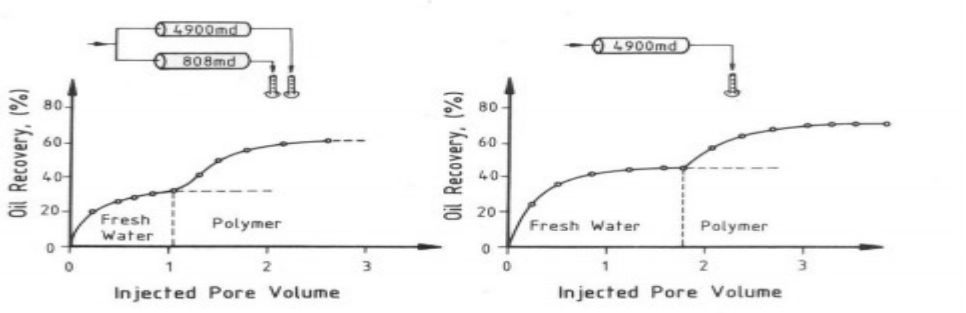

Figure 8: The polymer solution effect regarding the heterogeneous reservoir.

Figure 8 above presents the flooding experiment results by Sandiford, which define a system of two parallel flooded cores of various permeability. Due to the polymer flooding, the oil recovery is higher than the one flooded in only one core with uniform permeability.

2.3 Foam Flooding

2.3.1 Introduction

Foam has many useful features like an injection fluid for EOR.A different crucial aspect where the foam has been used for example; hydraulic fracturing, acidizing matrix stimulation, gas and water shut-off, but the most relevant application is gas mobility control during injection to relieve the opposite reservoir heterogeneity effects, gravity override and low gas viscosity. There are several manners in which the movement of gas is decreased, first by the apparent gas viscosity increasing, second by the trapping of the gas within the porous media, which reduces the gas relative permeability. The optimization of this application needs a good understanding of the foam physical aspects and its behavior under reservoir conditions. Although several theoretical and experimental types of research on foam and few field projects reported in the literature, there is no full research survey describing the experience and knowledge obtained through the foam utilization. The purpose of this work is to give an important survey of the literature available on the foam application for improved oil recovery. From thermodynamic prospective the foam is not stable, thus; it is not treated as one phase. The thin liquid layer which separates the gas bubbles is known by “lamella.”

The force required to sustain the lamella is described as disjoining pressure. The disjoining pressure is combination of several forces such as van der Waals force, protrusion, and adsorption and hydration effects. The foam texture is the lamella number per unit area [5]. Despite that, the foam texture plays a critical part in foam properties, there is no straightforward procedure to estimate this parameter inside porous media during the displacement process. In order to identify the foam, the pressure gradient is used. [6] [7] Foams are classified into two categories: weak foam and strong foam. On one hand, the weak foam texture is thin, where it has a coarse texture and drives to the low-pressure gradient. On the other hand, the strong

foam has a thick texture, which leads to a high-pressure gradient. Figure 9 shows types of foams.

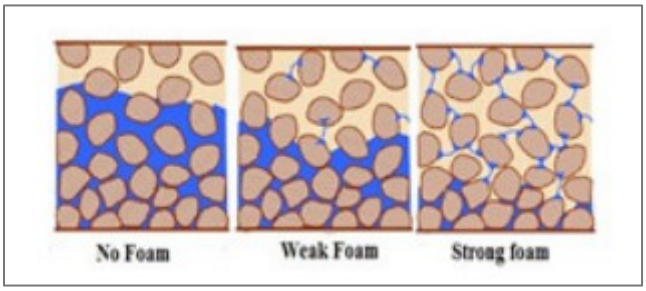

Figure 9: Types of foam texture

As cited before the foam isn't stable. Therefore, the lamella is unstable. It coalescence destroys the foam. The lamella coalescence is the result of surface free energy changing caused by an alternating interfacial area between immiscible phases. As it was stated in the previous paragraph disjoining pressure sustains the lamella, and the lamella will collapse when this pressure reaches the maximum value. This maximum disjoining pressure value is associated with capillary pressure which is described as “limiting capillary pressure” (pc*).

2.3.2 Foam Generation Mechanism

Using two-dimensional sandstone pore structure scratched in a silicon wafer with an accurate grain shape, size design, the aspect ratios of pore-level foam generation of pore-level, sweep efficiency, and propagation were reflected. The three mechanisms of foam generation will be explained in the section below for details.

- **Snap-Off**

When a gas-bubble front penetrates a pore throat and jumps out of the downstream side, snap-off occurs. (This phenomenon is called Haines jump or a rheon.). As the gas bubble expands, the capillary pressure reduces, causing a pressure gradient in the liquid phase for flow from the surrounding liquid into the neck of the pore throat. The incoming fluid, which is collected at the construction of a collar, and if the capillary pressure drops below a critical value, the liquid eventually snaps off a gas bubble. Several studied about the process of capillary snap-off of a no wetting phase in porous media were done. It is widely believed to be an efficient foam-generation mechanism. Compared to the leave-behind mechanism, snap-off generates a separate gas bubble, injecting the gas into discontinuous form. Also, it can happen frequently occur at one site, so snap-off at a single site can affect a relatively significant portion of the flow field. The snap-off mechanism affects the gas phase flow properties by raising the gas phase discontinuity and by producing lamellae. The formed gas bubbles can lodge at some spot in the porous medium, thereby blocking gas pathways and causing an effect similar to

lamellae resulting from the leave-behind mechanism. Alternatively, the generated bubbles may flow. The resistance to gas flow in the bubble or discontinuous form through porous media is considerably higher than the flowing gas as a continuous phase; apparent viscosities for foam movement via porous media on the order of 100 mPa· s [100 cp] are not uncommon. Nonetheless, snap-off generates stable foam.

- **Lamella Division**

Lamella division is different from the other mechanisms in that it needs a moving lamella; in other words, some foam generation must have already occurred.it is more appropriately a shaping or subsequent generation mechanism. This mechanism can happen wherever a lamella approaches a branch point in the flow field. At such a site, the gas which is front of the lamella can flow either into two or more channels downstream of the branch point or into only one of the downstream channels. In the latter case, no division occurs; either the lamella or the bubble is altered. However, in the first instance, which is illustrated schematically in Figure 10, one lamella is split into two or more lamellae. A sequence of frames in which this mechanism is realized is given in Figure 11. The gas bubble indicated in Figure 11a is forced to flow into the branch point shown in Figure 11 b. As the lamella at the rear of the bubble approaches the branch point, the bubble divides into the two bubbles shown in Figure 11c.

The features of this division lamella mechanism are very similar to those of the snap-off mechanism: a separate gas bubble is generated, which can either flow or block gas pathways, the mechanism can occur several times at one site, and it is observed to be more significant at greater gas velocities. Thus, it's hard to distinguish between the Lamella-Division and snap-off mechanisms without looking at the pore-level mechanics. Because of this, in later sections of the chapter, the fine foam generation occurs almost by a combination of the snap-off and lamella-division mechanism is indicated simply as generation by snap-off.

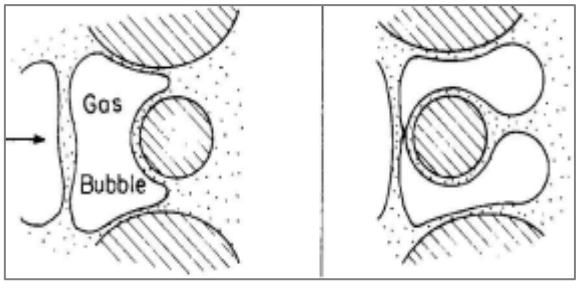

Figure 10: Schematic of the lamella-division mechanism.

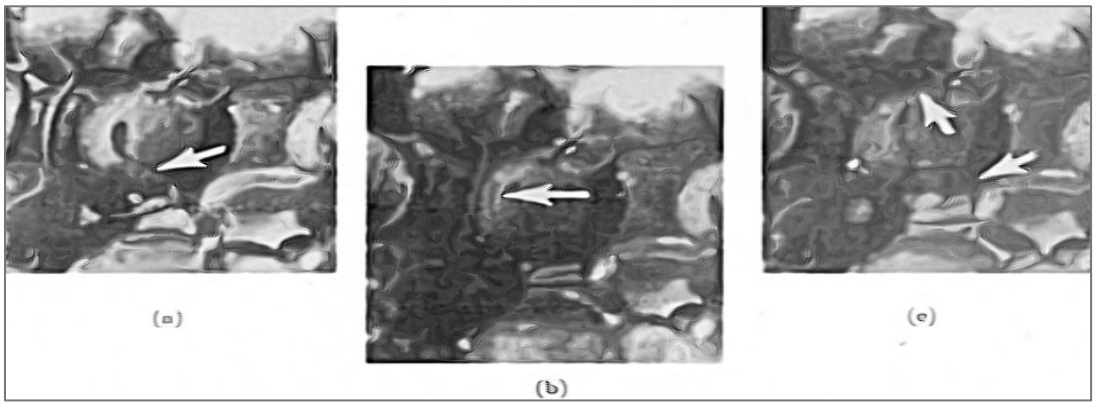

Figure 11: Three movie frames in sequence, showing a bubble undergoing division. The gas bubble indicated in (a) approaches the branch point in (b). As the lamella at the rear of the bubble is forced into the branch point, division occurs, and the two bubbles shown in (c) are made.

- **Leave-Behind**

The leave-behind mechanism, which is shown schematically in Figure 12, is the dominant foam-generation mechanism below a critical velocity inhomogeneous bead pack. As gas invades a previously liquid-saturated area, it penetrates through the multiple interconnected flow channels. From different directions, two gas fronts approach the same liquid-filled pore space, when this occurs, the liquid in the pore space is pinched into a lamella by the two fronts. When this occurs, the liquid in the pore space is squeezed into a lamella by the two fronts. If sufficient surfactant exists in the liquid phase, this lamella may be stable; if not, it ruptures. It is necessary to understand that this mechanism does not need the two gas fronts to converge simultaneously on the site; they can appear at different times and squeeze down the lamella as the local capillary pressure rises. In highly connected underground porous media, it is probable that this mechanism occurs very frequently. The outcome is the formation of a vast number of lamellae blocking gas pathways. It is known that the lamellae decrease the relative permeability to the gas phase by blocking flow channels and creating dead-end paths. Thus, leave-behind produces a relatively weak foam. There are a few significant consequences of the leave-behind mechanism on the foam that is formed. First, no separate gas bubbles are formed by this method of foam generation, so the gas remains as a continuous phase. The lamellae that are created provide a potential source for flowing lamellae. Another consequence is that once a lamella generated by leave behind ruptures or flows out of the site, a second

lamella cannot be made at the same location by this mechanism unless liquid reinvades the region.

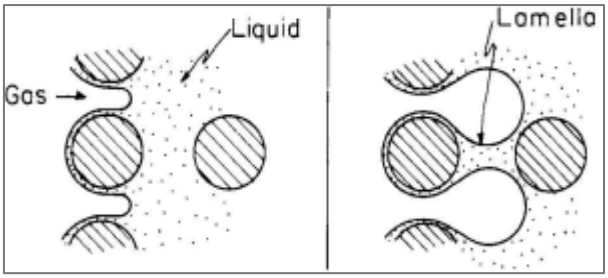

Figure 12: schematic of the leave-behind mechanism.

2.3.3 Foam Termination Mechanisms in Porous Media

In the absence of oil, the lamella rupture by two methods where both result in the generation of one large bubble rather than two smaller bubbles that initially filled the pore body. Nonetheless, the first one occurs via a fast-physical mechanism while the second occurs via a slow diffusion mechanism. The two processes are defined in the next part.

- **Capillary suction coalescence**

The lamella coalesces when the bubbles are immediately spread over large pore bodies. For gas flow rate and capillary pressure, the pore body-throat with high ratios works as termination spots. As the capillary pressure and gas velocity rise in the porous medium, an increasing number of throat-body configurations become termination spots.

- **Gas diffusion coalescence**

Static or trapped bubbles can burst by a gas diffusion process. Usually, the gas spreads from small bubbles (highly curved) to larger ones (less curved) through the middle lamella. Finally, the smaller bubbles disappear along with the typical lamella.

- **Foam quality**

The foam quality is characterized by the gas volume to total volume ratios which is presented in Figure 13. This parameter is a sign to indicate the foam quality (low or high foam quality). The transition foam quality (fg) is known as the foam quality corresponding to the maximum pressure gradient value. This transition foam quality depends on surfactant type and its concentration, in addition to the rock permeability and type. The foam generation mechanisms are classified into three methods; first, leave behind, where the lamella derelict behind as the gas invade into the surfactant solution for example; during the drainage process, the second method is the snapped-off; the gas driving force on gas-liquid interface causes the bubble

formation, also the capillary fluctuation leads to the bubble formation, the last one is the lamella division, where The pre-existing bubbles are separated into many at pore crossing due to pressure gradient. These three mechanisms are demonstrated in Figure 13.

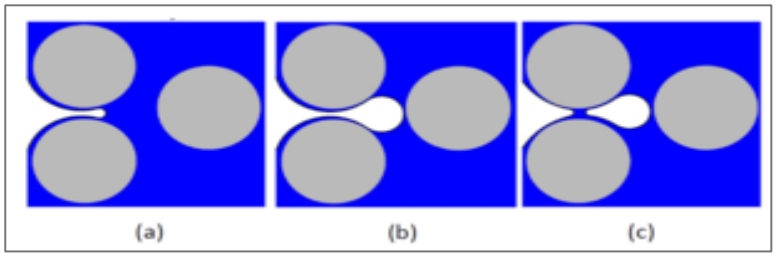

Figure 13: Snap-off mechanism. a) Gas invades the pore body, b) The entrance of the gas to the pore body, and c) wetting fluid moves back to snap off the gas thread.

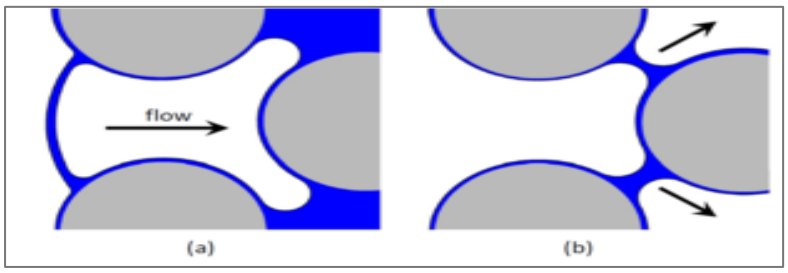

Figure 14: Lamella division in porous media.

- **The permeability effect in Foam mobility control**

The most significant rock factor affecting foam propagation in porous media is permeability. The chemical slug size and quality of the injected foam are the primaries process-designs parameters that affect both foam stability and rheological behavior. The experiments results show that foam decreases gas mobility in high permeability media than in the low one. For example, Djabbarah et al [9] investigate CO2 displacement ability using parallel one-dimensional porous medium with various permeability values. For example, Djabbarah et al. [9] investigate CO2 displacement efficiency with foaming agents in one-dimensional parallel porous medium with various permeability. They discovered that the injection of foam cause increasing the flow resistance in high permeability layers and at the same time the injected CO2 deflected to less permeable zones.

Bertin et al. [9] create a heterogeneous porous medium with permeability contrast of about 70:1. In the case where the foam is not being used, a small amount of gas moved into the low

permeability sandstone core, while in the case where the foam was used, a large volume of injected gas was diverted. Nguyen et al. (2004) [9] researched foam flow in heterogeneous cores using high- resolution computed tomography (CT) to investigate pore-scale phenomena. They inspected that when there is a transient liquid displacement, the foam front passes in more steady and uniform way in high permeability layers. Tsau and Heller (1996) [9] further discovered that the enough increasing in foam viscosity occurs with increase in the permeability and this foam behavior is called" selective mobility reduction". This would help to obtain better conformance control in foam flooding process.

3 Micromodel: Overview

Early micromodel experiments used capillary tubes with different diameters and lengths to study the miscibility or displacing process of various fluids or phases. Those models consist of two glass plates with a narrow space in between allowing the fluid to flow. Later, this area was filled with glass beads to build a kind of artificial porosity and permeability. They were simple models not able to count the rock properties and pore geometries. To study the flow behavior pore scale in the more realistic method, the micromodels were invented. The porous media patterns were etched on a silicon or glass surface. Micromodels have been widely used to investigate more about the flow behavior of multiphase flow, solution gas drive, contaminant hydrogeology, oil-foam interaction studies, etc. The patterns used in the porous media fabrication were prepared from thin sections. Many cases have geometrically constructed from series of repeatable simple or complicated geometric configuration. Nonetheless, since the micromodels represent a two-dimensional porous medium, flow problem and extrapolation of results to the three-dimensional flow problem in the real porous medium have to be done with caution. It has also been observed that a no uniform etch depth in the micromodels may lead to snap-off situations not consistently predictable with the flow behavior. Another constraint of the micromodels is concerning the dimension of the lower macroscopic connectivity and coordination number. [6].

3.1 Micromodel Fabrication

Since the earliest prototypes were introduced [7], micromodels have rendered fluid flow visualization via microchannel networks. An increase in the number of multidisciplinary studies that utilizes microfluidic tools to understand the mechanisms in more detail. This purpose needs additional micromodel type improvements and adjustments depend on the underlying method conditions. Therefore, model fabrication techniques and alternative materials have been examined largely. There are different transparent materials that can be applied in micromodels fabrication process such as glass, poly (methyl methacrylate) (PMMA), and quarts. Because of the relatively higher thermal and chemical resistivity and it is availability, the glass substrate is more common in micromodel tests. The prototyping methods for glass micromodels that are generally suggested in the literature can be classified as follows: the Hele-Shaw and glass-bead models [8], optical lithography [9], etching, stereo lithography [10], and soft lithography [10].The etching process can be named dry or wet based on the chemical, etchant agent, or plasma. The Figure 15 shows the workflows of the wet etching fabrication are masking, etching, and bonding. During masking, a glass plate (with or without primary metal coating) is coated by a thin layer of photoresist in a spin coater device. (Figure 15 a) Following, on a transparent element (photomask), the wanted network design is printed. And

later it is exposed to ultraviolet (UV) light via the photomask in a mask (Figure 15 b). Consequently, the plate is submerged in the developer liquid .While photoresist growth the sections where the photoresist is exposed through UV convert to solvent in the developer and the unexposed sections remain unsolved lastly the solvent flow pipes are taken away by the compressed liquid to form the network mask on the glass for the photoresist metal mixed layer then a diluted nitric acid solution is applied to extract the residual mineral sheet inflow channels. The condition of the pattern using lithography is significantly limited by the execution of the photoresist's layer method making an efficient layer with constant bonding and consistent density is highly sensible to the selection of layer substance as strong as the layer method. The etching step introduces an acid solvent as a chemical tool that separates the silicon-based

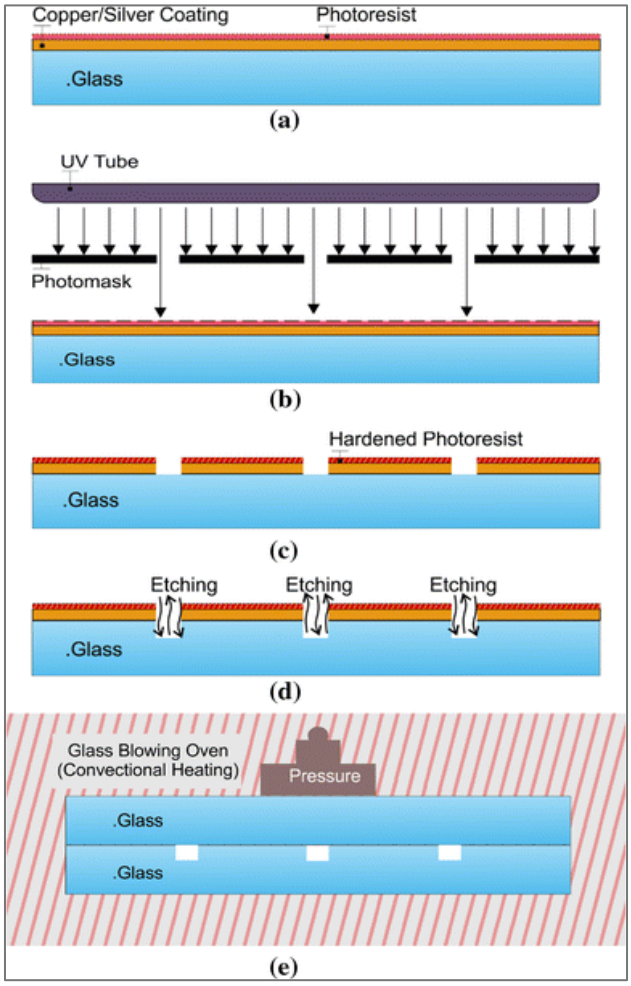

Figure 15: The steps of wet etching fabrication. a) Photoresist coating on a glass surface with (or without) metal layer. b) UV light radiation through the photomask. c) Washing developed photoresist mask (and the metal layer). d) Wet etching in the HF solution.

elements like silicon wafers or glass quartz and produces flow channels < 1 mm in unmasked sections the tool happening in this method is a simplification of silicon oxide dissolution to hydrofluoric acid the following equation represents the etching effect.

$$SiO_2 + 6HF \rightarrow H_2SiF_6 + 2H_2O \quad (1)$$

At the same time with reaction. (1), the present oxide elements like $Al_2 O_3$ and CaO (impurities) react with acid and generate insoluble products in the HF solution. These products form an unwanted film on the etching surface, this film exhibits the main difficulty in the chemical etching method such as etching rate drop over time and undesired roughness disposition on the surface. The final part of this procedure is bonding the etched glass plate with another flat plate (Figure 15e). Several bonding methods such as eutectic, adhesive, and thermal bonding have been developed based on different applications for the micromodel [11].

3.2 Porosity Calculation

The different properties (lengths, width, and area) of porous network grains were measured using “Rhinoceros®”. The total grain area was subtracted from the bulk area to determine the porous medium areal porosity. All the utilized microfluidic chips were manufactured by a wet etching method, liquid acid erodes the glass in an isotropic way. Hence, pore walls will not be vertical. The calculated volumetric porosity based on the pore volume stated by the manufacturer is presented in Table 2.Figure 16 shows the documented design rules given by Micronit. Curved walls create a difference between areal and volumetric porosity and fluid saturations. Nevertheless, satisfactory experimental outcomes are achievable using merely areal properties.

Network Type	Channel Width [µm]	Channel Height [µm]	Total Internal Volume [µl]	Rock pore Volume [µl]	Permeability [Darcy]	Porosity [%]
Uniform	50	20	5.5	2.1	2.5	52
Random	50	20	5	1.6	1.6	40
Physical Rock	50	20	5.7	2.3	2.5	57

Table 2: Measured dimensions and determined areal features for three available network models.

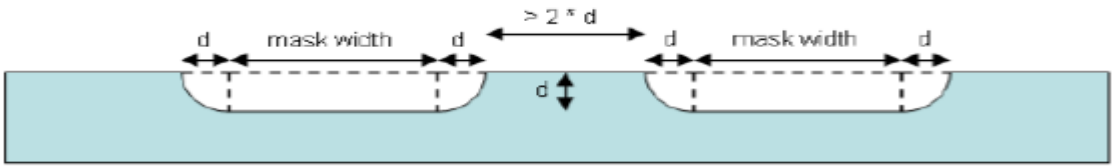

Figure 16: The channels and pore networks cross-sectional view documented by Micronit.

3.3 Grain Size Distribution

Main six grains sizes were detected in the micromodel, varying from 50 to 400 mm^3 in the area, with mean areas are between 144 and 3144 mm^2 (see Figure 17) A pore structure picture of the microfluidic is observed in Figure 17, which has the dimensions of 227 X 171 mm. From this specific image. The data regarding the different grain size area and their frequency can be seen in Figure 18.

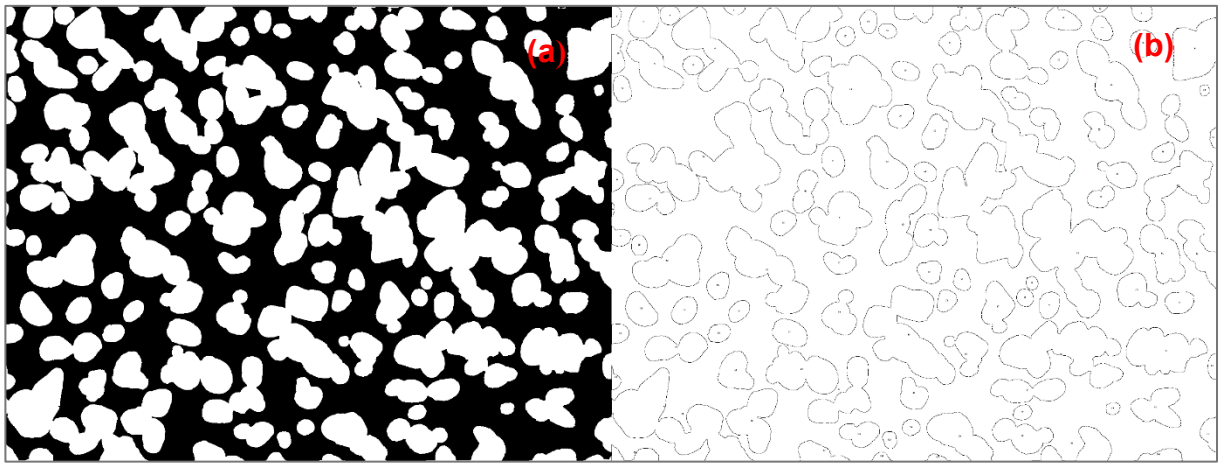

Figure 17: The micromodel segment with dimensions of 227 mm X 171 mm. Pores and pore throats are indicated in black while the grains are indicated in white in an image (a).

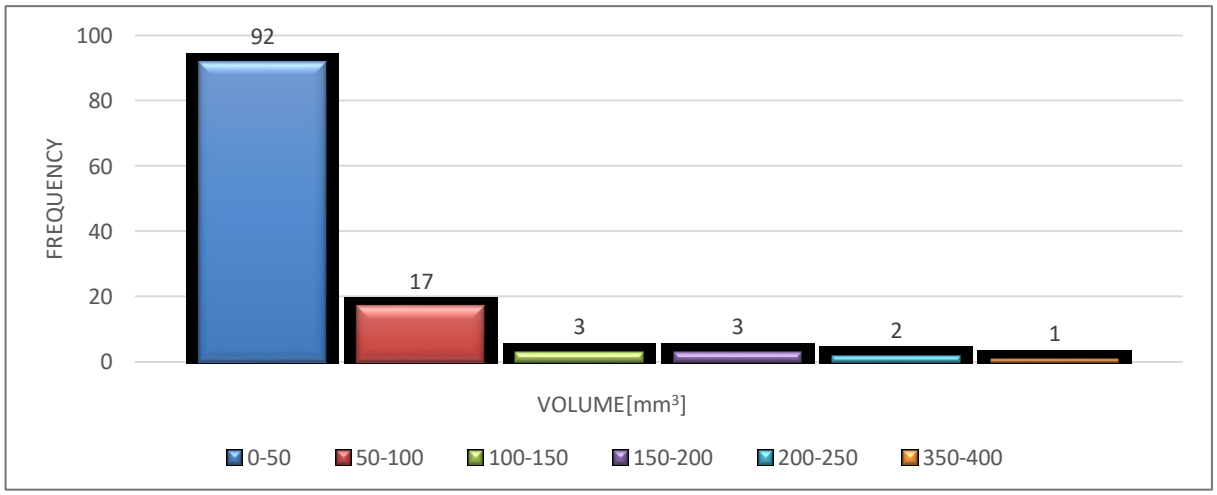

Figure 18: The grain size distribution at one location in the micromodel.

3.4 Chip Holders and Connection Kit

As the name indicates, it holds the microchip and connects the tubing to the outlet and inlet of the micromodel's holes. There are several types of chip holder types, but only one chip type holders were used in this work:

- Standard chip holder, which is made of aluminum. This device can be used at pressure and temperature up to 10 bars and 80°C, respectively.

Figure 19: Aluminum chip holder

4 Materials and Experimental Apparatus

This chapter will present a general overview of the materials used for the experiment and for assembling the supporting data. The apparatus consists of three parts: the data gathering system, the injection system and the chemical product for EOR.

4.1 The Data Gathering System

4.1.1 Microscope and Camera

- Motic's new AE2000 Microscope is created for, routine-clinical, university, and laboratory settings. The model's essential applications are offering excellent image quality for research purpose. In this work, the microscope with camera mounted on it used to surveillance the pore spaces via a camera. Both pictures and videos are taken through this adapter. Four different magnifications were used to observe the micromodel. The obstacle in this work is even with the lowest magnification objective, a full range image of the microfluidic chip cannot be captured. Moreover, due to uneven illumination, captured images showed a tapered brightness that caused difficulties in further image analyses.
- The Moticam 5 characteristics a 5MP live resolution capability, is used to collect pictures at micro and meso-scale. High magnification micro-images are taken with the support of the microscope.

Figure 20: Motic AE2000 inverted microscope with digital camera

4.2 Injection System

Two major parts build up the injection system:

- Syringe pump (for pumping water, polymer, foam and surfactant)
- Vessels for water, brine, polymer, oil, foam, and surfactant.

4.2.1 Laboratory Syringe Pump

For the pumping procedure, the Laboratory Syringe Pumps is inexpensive and straightforward to use. They are suitable for a large range of experimental and teaching objectives. In syringe pumps, a stepper motor affords a continuous screw motion (screw drive) on which the pusher block is set; it could hold small or big syringes up to 60 mL, with a maximum pumping rate of 1257 mL/hr with a 60 mL syringe [12].In this experiments, Era NE-300 syringe pump (Fig 22) was used to inject the different fluids solutions. The specification of the syringe pump is described in

Table 3 below:

Syringe Sizes	up to 60 mL
Number of Syringes	1
Moter Type	Step Motor, 1/8 to 1/2 step modes
Steps Per Revolutions	400
Stepping (max. min.)	0.21µm to 0.850µm
Motor to Drive Screw Ratio	15/28
Speed (max. /min.)	3.7742 cm/min / 0.004205 cm/hr
Pumping Rates	1257 mL/hr with 60mL syringe, to 0.73µL/hr with 1mL syringe

Table 3: The specification of The Syringe Pump.

Figure 22: The pump and plastic syringe were used in this work.

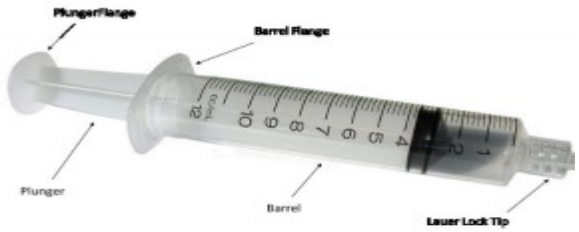

Figure 21: Plastic syringe and its main components.

The first thing to do before the pumping can start is to load the syringe with the fluid of interest, which is placed on the syringe holder block and being locked using the syringe clamp. Then the pusher block must be aligned with the syringe plunger flange. This alignment can be done by holding and pressing the drive button. Finally, for the setting of the syringe diameter (in millimetres), this could be either manually calculated or in most cases found in the original manufacturer´s catalogues. The used syringes inner diameter that been used in this research are listed in Table 4.

Manufacturer	Material	Volume [ml]	Inner Diameter [mm]
B. Braun	Plastic	10	15.96
	Plastic	3	9.71

Table 4: Plastic syringe and its main components

4.2.2 High Precision Balance

Preparation of polymer solutions demands a high precision scaling device. A Kern EG series scale with three decimal precision was applied for this object. (See Figure 23).

Figure 23: High precision balance

5 Experimental Procedure

The main experimental procedure and preparation purpose was to create a same or at least very similar initial conditions for every experiment. Therefore, each experiment had the same workflow:

- Clean micromodel holder and micromodel
- Saturate micromodel with water
- Saturate micromodel with oil (takes pictures to determine S_{wi})
- Start the flood with the concerned product for each experiment or water and take pictures during the flood and micro scale pictures after breakthrough

In the next section of the thesis will discuss the specific work for each steps of the experiment.

5.1 Clean Micromodel Holder and Micromodel

The cleaning of the micromodel holder is the first step of an experiment. When pumping the different types of a solution through the micromodel, small precipitations could form at the inlet ports of the holder. These small particles may flow during the next experiment and plug the pores, which leads to change in initial conditions. By using a vacuum pump, isopropyl alcohol (IPA), toluene and water the two entry ports of the holder and the O-rings can be free from oil and solutions. When cleaning micromodels, the following method is used.

- Step 1: Use the isopropanol (IPA), around 150 pore volumes (3 ml) at constant flow rate, to eliminate the residual oil and clean with isopropanol. In this configuration, water pushes IPA into the micromodel and micromodel holder assembly. Once IPA begins to flow out of the outlet port of the inlet fracture, cap this port. Keep pumping IPA at 1mL, or until there is only immobile oil in the micromodel.
- Step 2: Pump with toluene (200-240 pore volume) at constant flow rate to get rid of the remaining residual oil; once toluene is recognizable at the outlet port of inlet fracture. Continue pumping at the same flow rate until micromodel appears to be clean.
- Step 3: Pump the water to remove the toluene. Using the microscope, Check if the streaky toluene spots remain, to guarantee that there are no visible spots in the micromodel. If any residual oil remains in the micromodel, repeat steps three and four as necessary.
- Step 4: Pump with IPA: Repeat step 2, when the micromodel is 100% saturated with IPA. Any toluene spots remarked in step 3 should be removed by the IPA. Finally, the micromodel is clean and ready to be fully saturated with oil.

5.2 Saturate Micromodel with Oil

After cleaning the micromodel or using a new one, it must be saturated with water (300 pore volume which it is approximate to 6 ml). Then the oil is injected. The experiment set is presented in Figure 24.

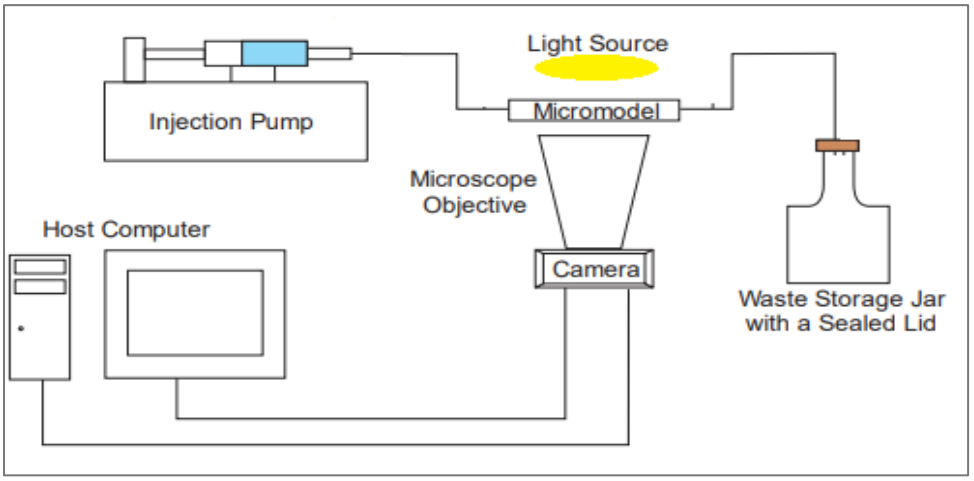

Figure 24: Experimental setup for water saturation

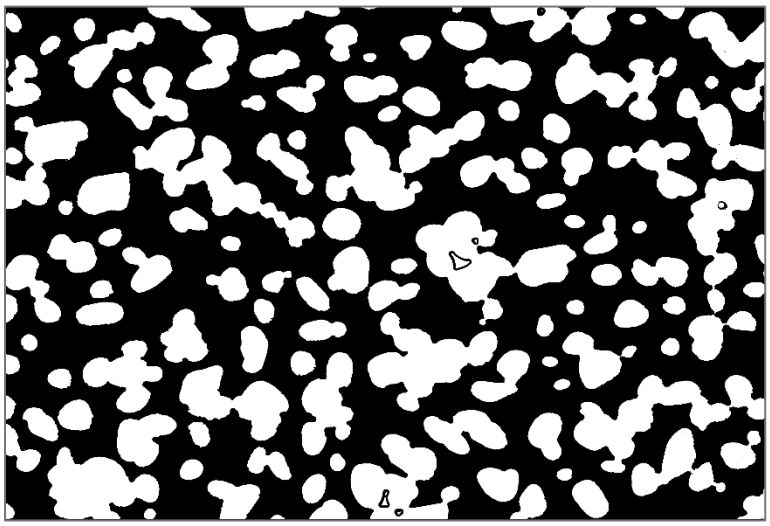

Figure 25: Captured image using microscope: after segmentation to illustrate the grain (white color).

5.3 Crude Oil Properties

The oil field of Matzen is located 20 km northeast of Vienna in the Vienna basin, which consists of numerous reservoirs the 8th and 16th Torton Horizon (TH) reservoirs are the two principal prolific horizons of the Matzen field, in this thesis, only the 16th was under investigation for the different solutions flooding. Oil samples from 16th Torton reservoirs were provided by OMV. The Table 5 shows the essential properties of the oil sample.

	Oil Sample 1	Oil Sample 2
Well	Schönkirchen 446	Bockfliess 112
Reservoir	8th Torton Horizon	16th Torton Horizon
Sampling date	17.11.2015	19.10.2016
Sample-ID	CHE20155426	CHE20165728
TAN [mg KOH/g oil]	1.96	1.56
Density @ 20 °C [g/cm^3]	0.9306	0.9070
Density @ 15 °C [g/cm^3]	0.9339	0.9104
Viscosity @ 20 °C [cp]	331	80
API ° (8)	19.88	23.79

Table 5: Oil samples properties

6 Experimental Setup and Methodology

6.1 Experimental Procedure for Surfactant

The type of surfactant used in this work is Poly (ethylene glycol) (12) tridecyl ether with a linear formula $C_{13}H_{27}$ $(OCH_2CH_2)_n$ OH, n~1.A non-ionic surfactant was used as pure surfactant material. It has been already implemented to separate oil and water from each other and to mobilize the trapped oil in an oil field application. In these flooding experiments, the surfactant was made by dilution of pure surfactant using distilled water. A surfactant solution was made by mix 0.5 ml of surfactant with 500 ml of deionized water which create a solution with 0.1 wt. % concentration. The injection rate is about 0.01ml/hr. Micromodel was filled with oil saturation. A secondary and tertiary flooding was investigated.

6.2 Polymer Flooding Experiment

In these experiments, deionized water and xanthan gum were mixed together to create aqueous the solution. For an appropriate mixing, the stirrer was set up at speed high enough to create a very strong vortex, which is around 9-10 PRM. Then, the weighted polymer is combined slowly by sprinkling it into the wall of the vortex. After 2-5 minutes of stirring, the RPMs are decreased to5-6 RPM, and at this rate, the solution is stirred for four more hours. The mechanical stirrer also heats up the plate to enhance the dissolution process. Frequently, few particles do not dissolve, so the solution is filtered using a filter with a mesh size of 15 µm. In this experiment a mix of 100ml of water and 0.5 mg of xanthan gum, a solution with concentration of 10^{-3} wt. % was prepared.

6.3 Foam Experiment

To generate foam the Surfactant alternating gas (SAG) flooding was conducted. As the name indicated; the surfactant slug is first injected and follows by gas slug injection.

1. The micromodel is filled with water.
2. Injection of 2 ml of surfactant (Poly (ethylene glycol) (12) tridecyl) with 1wt% as concentration.
3. In this experiment air was used as injected gas, with size slug of 10 cm^3

This experiment results in bubbles generation as shown in the Figure 26 below:

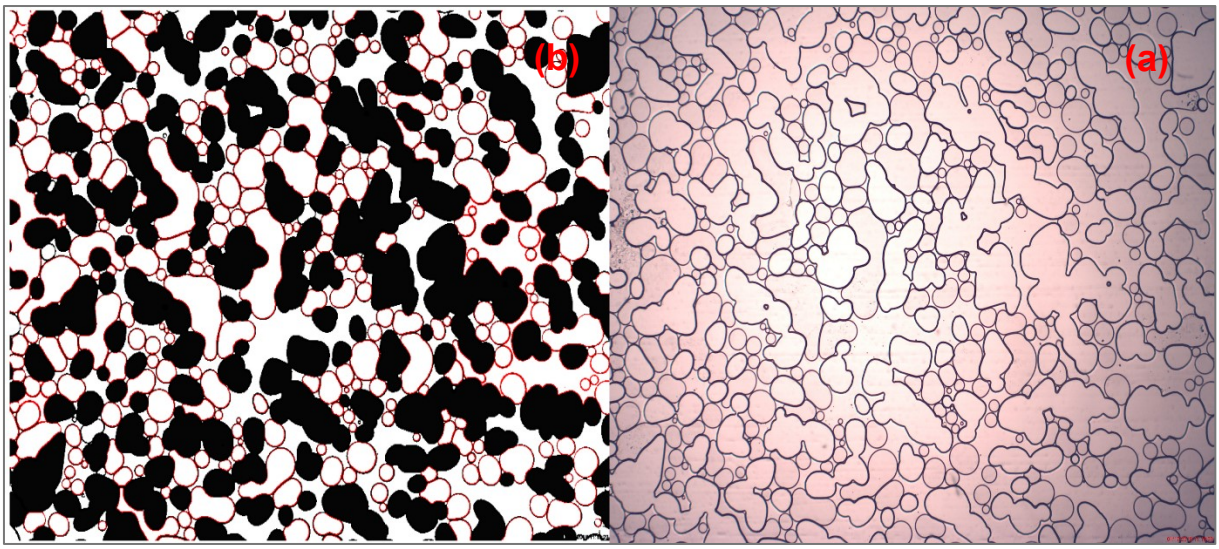

Figure 26: Bubble Generation using SAG method; a) original image, b) the processed image shows the grain in black color and the edges of bubble are indicated in the red.

6.4 Photo Capturing and Complete Range Image Preparation

During the floods of the different experiments, digital images of the microfluidic chip were captured by the microscope aid and a digital camera. As mentioned before, because of the microscope limitation, it was not possible to capture the full range images of micromodel. At the end of each experiment, another microscopic was used to capture photos covering more significant areas of the microchip. These images were used to measure the recovery factor.

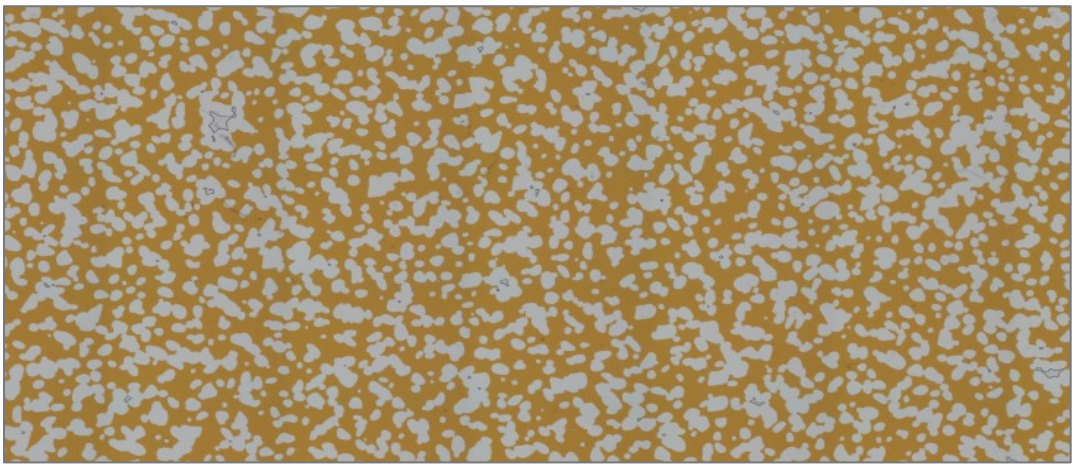

Figure 27: prepared full range picture (the microchip is saturated with oil).

7 Image Analysis

Several steps should be done first, so the recovery factor can be measured. After taken images using the camera, this image should be converted to binary (black and white), where the residual oil is presented by black pixels. In the processed images, the contrast is very high between the oil and the water, which make it easy to distinguish between the two phases. In the next section, the executed image analysis and validation procedures are described concisely. In this research, the software ImageJ was used as the image-analysis tool for several reasons, for example, it is a free and open program with many plugins and scripts that are very extensible, which are able to perform a wide variety of tasks.

First, it is important to explain some essential expressions and commands regarding image analysis, before starting with the procedure description.

- Erode: extracts pixels (white) from the edges of objects in a binary image.
- Dilate: combines pixels (black) to the sides of objects in a binary
- Subtract Background removes smooth continuous backgrounds from images. This feature is beneficial when analyzing images with an uneven background light distribution.

7.1 Areal Porosity Measurement Using Oil Saturated Microchip Image

Images of 100% oil saturated microchips were used to determine the value of areal porosity in the micromodel.

To start the channel color should be split. These results in three individual channel images: red, green and blue. Then the background must be subtracted, as the background light is not evenly distributed and gives rise to generating incorrect binary images.

The last step is to adjust the black and white threshold values to obtain a suitable binary image. Sometimes it is likely to capture poor quality image, it is recommended to recheck the pictures that were not taken in the same conditions (such as lighting, chip holder position) before the threshold.

Finally, to measure the ratio of the white pixels (grain) to the black pixels (oil) pixels. It needs only the "measure" command in ImageJ. Before this, and after making the binary image it required to press "Dilate" and "Erode" twice to diminish the visible artifacts. Considering the microchip was saturated with oil (black pixels), it was possible to calculate the fractional area the fractional area (black to white) which is equal to the areal porosity; the measured value of the porosity is 53%.

8 Results and Discussion

This chapter exhibits observations, conclusions, and outcomes of the previously detailed experiments. In each test, ultimate residual oil saturation was measured by analyzing both the full-range images and presentative area, so two recoveries factors were calculated. Each different experiment was investigated in detail, and the results were compared in terms of recovery factor, sweep efficiency. The average recovery factor for the flooding experiments was calculated applying the equation presented below:

$$RF = \frac{Volume\ of\ produced\ oil}{Volume\ of\ oil\ initially\ in\ place} = (1 - \frac{A_{oil-residual}}{A_{oil-initial}}) \times 100 \quad (14)$$

The determined recovery factors for the different experimental scenarios are present in

Table 6. The following outcomes were extracted from this table

	Concentration	Secondary Flooding	Recovery Factor	Tertiary flooding	Recovery factor
Surfactant flooding 1-1 Poly (ethylene glycol) (12) tridecyl	0.1 wt.%	✓	56% 66% 61 %	✓	70%
Polymer flooding 1-2 Polymer flooding 2-2 [Xanthan Gum]	10^{-3} wt. /vol % 2.10^{-3} wt. /vol%	✓	66% 71%	✓	84%
Polymer-surfactant flooding [seq]1-3	Surf: 0.1wt. Poly:3.10^{3}wt%		58% 67% 63 %	–	
Polymer-surfactant flooding [co-inj] 1-3	Surf: 0.1wt. % Poly:3.10^{3}wt./vo	✓	55% 67% 61 %	–	
Water flooding 1-5	Deionized		61% 57% 59 %	–	

Table 6: Calculated ultimate oil recovery for each experiment

- As
- Table 6 shows, five experiments were conducted applying different chemical flooding solutions, under the same conditions, to look at the mechanism for oil recovery and to compare which solution yields to a high value of recovery factor. The first experiment was the water flooding, where the micromodel was filled with oil and then flooded by water at 0.01 ml/h. In the end of these experiments, the lowest recovery factor observed was 59%

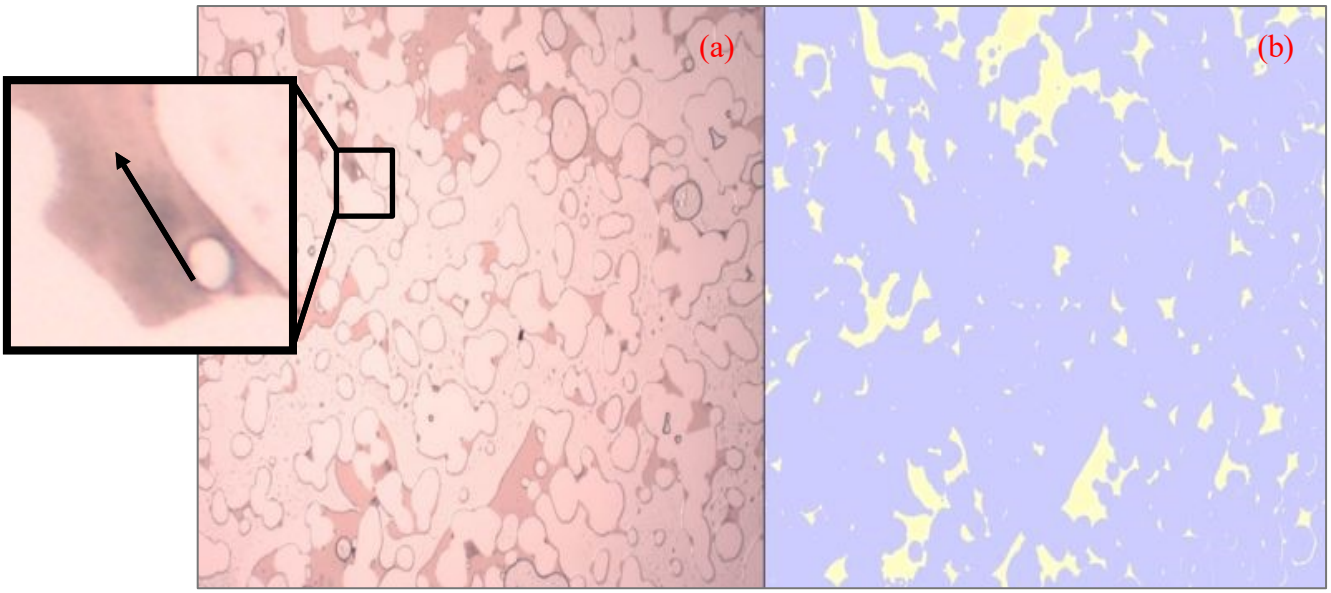

compared to the other experiments.

In the water flooding experiment; the formation of residual oil clusters with different sizes was observed. The variation of clusters size is usually dependent on oil-water IFT, pore geometry, pressure gradient, and likely, on interfacial film characteristics. As water enters the porous media, the increase in water saturation causes the continuous oil filaments to be ruptured which leads to the creation of an oil-water transition zone. Also, micro-emulsions were observed. The macro-emulsions mostly made by the water phase snap off, and by the coalescence. At the interface of oil and water, the emulsions were generated during both the oil and water flooding. The micro emulsions are stable as shown in Figure 28 (see the black box) and are movable by the flowing current (the black arrow indicates the direction of the flow).

Figure 28: A detailed image of oil clusters (light color) during water flooding; a) the original image, b) the processed image.

- To understand how surfactant flooding can enhance oil recovery, it is essential to observe the distribution of remaining oil. Hence, a microscopic displacement was made using

micromodel. A surfactant flooding was performed where a solution of surfactant concentration of 0.1 wt.% was injected. It caused an improvement in recovery factor by 2% (average of 61%) compared to water flooding. The surfactant fluid strongly reduces the IFT between the displacing and displaced fluids. The low IFT heavily enhances the oil drops deformability and decreases the capillary resistance as presented in Figure 29 (a), (b) and (c), which facilitates their passage through the pore throat. First, the oil film front swells and disfigures along the flow path under the flowing system shearing force. On one hand, the oil film becomes sufficiently attenuated to move through the pore throat as Figure 29 (c). On the other hand, the micelles were formed and released the attenuated oil film solubilization and finally improved oil displacement efficiency, as exhibited in Figure 29. The surfactant is dissolved in both oil and water and is in balance with aggregates of the surfactant recognized as micelles as it is presented in Figure 30. Large pore volumes of the solution are mainlined into the micromodel to decrease IFT between oil and water. Oil

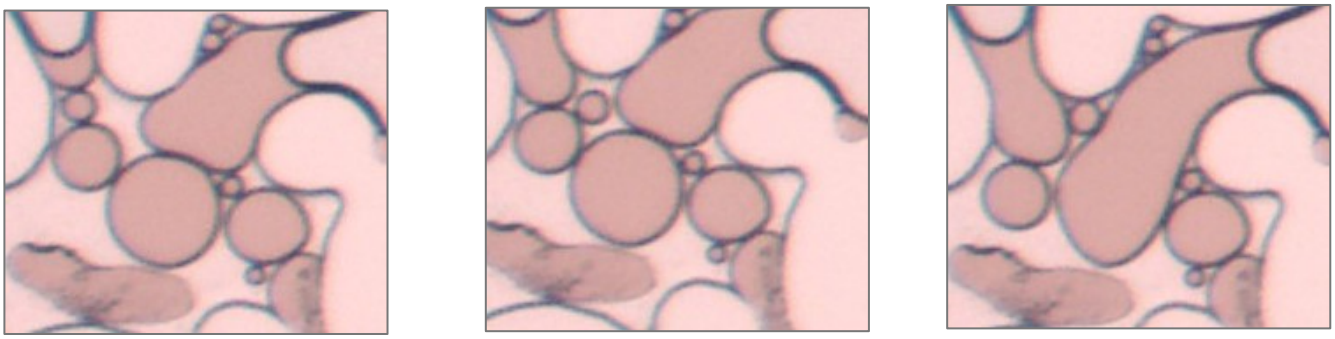

was deposited with the surfactant solution in the outlet part, while the remaining oil in the middle section of the micromodel was approaching zero when massive quantities of surfactant solution were flooded.

a b c

Figure 29: Microscopic images of the remaining oil movement during surfactant

Emulsion

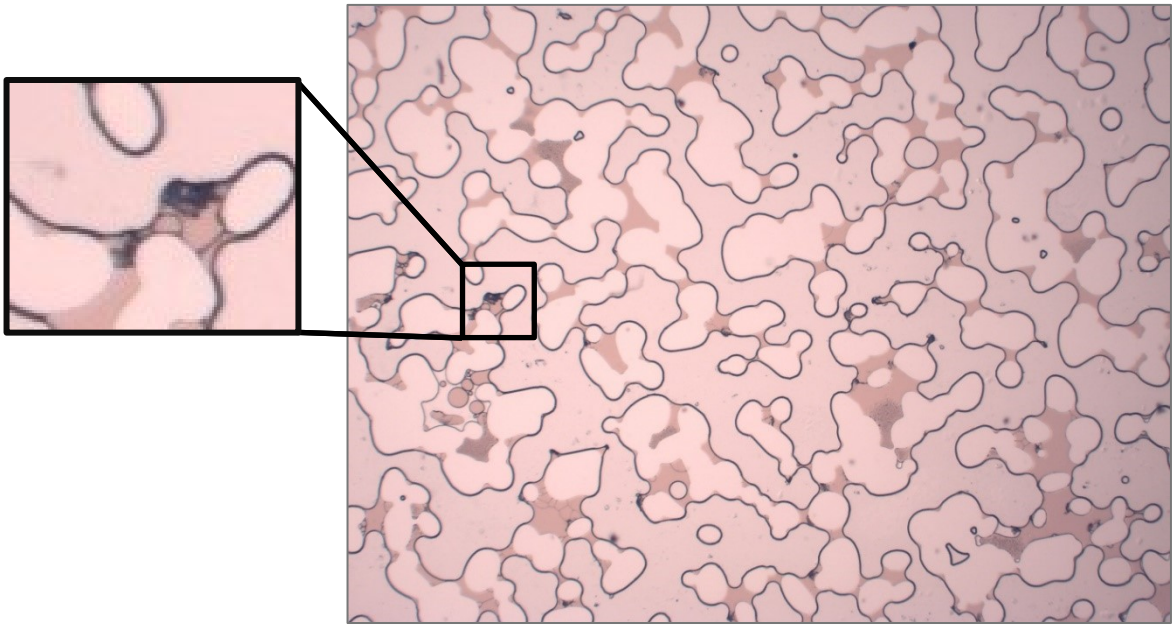

Figure 30: Detailed view (microscopic image) of Tertiary flooding of surfactant shows the formation of micro-emulsion.

in Figure 30. In the absence of the surfactant, the emulsion drops will rapidly coalesce, and the two immiscible phases will separate. In this case (the presence of a surfactant), the drops will be kinetically stabilized; that they will be prevented from coalescing by an energy barrier. Such emulsion systems do not form spontaneously. In the experiment 1-1, surfactant forms micelles in the oleic phase; the more hydrophobic the surfactant in the aqueous phase is; the less soluble the surfactant monomer is in that phase and the higher the tendency for the micelles to form in the oil phase. For appropriately formulated surfactant systems, the micelles can solubilize important portions of the oil.

- Both co-injection and sequence injection of surfactant-polymer were carried out. The microscopic displacement mechanism of the surfactant-polymer (SP) flooding was studied by experiments on the micromodel. After water flooding, a massive oil quantity was left in the micromodel while after the co-injection of surfactant-polymer flooding, little volume of residual oil has remained in the porous media. This means that the co-injection flooding has a much-improved sweep and oil displacement efficiencies. As a result, the objective of improving oil recovery was accomplished. The oil is slowly extended from a spherical to a cylindrical shape in the displacement direction, as demonstrated in Figure 31 (b) under the impact of shear stress and low IFT of the co-injection fluid.

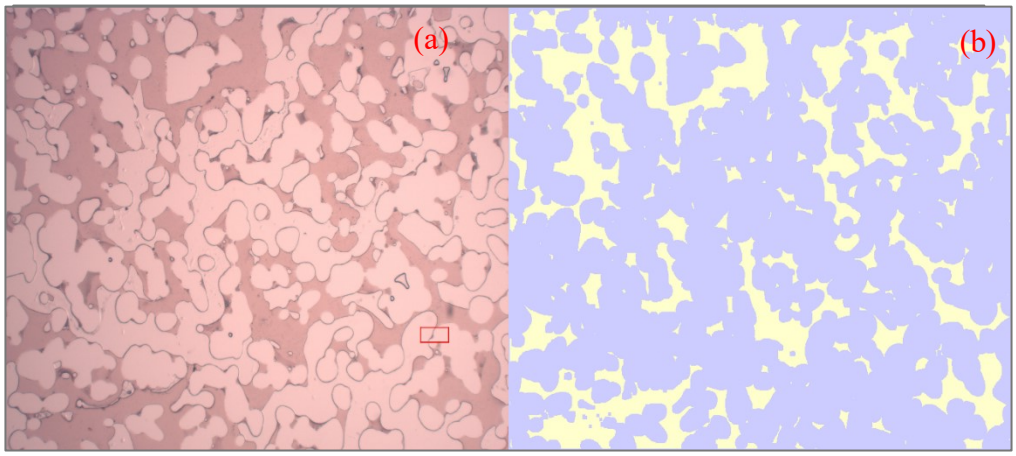

Figure 32: The different mobilization modes of the oil. (c) (d)

- Membrane remaining oil is attached to the pore wall. First, in the displacement path, the binary system implements a shear-pull force on the tailpiece of residual membrane oil, causing a little gap between the pore wall and the tail (see Figure 32 c-d, see the green box). As the flooding fluid slowly invades the tiny gap, the pore wall (initially lipophilic) will become hydrophilic, and the flowing fluid low interfacial tension will significantly cut the adhesion of the oil membrane to the pore wall, preventing the isolated

Figure 31: A microscopic view of oil clusters during surfactant injection: a) original image, b) processed image: oil clusters are shown in yellow.

oil membrane from connecting to the wall again, also the tail part is unattached from the surface, as the injected fluid is flooding, the process would go on. Eventually, the oil membrane would be separated from the pore wall and is hard to attach to the hydrophilic wall anymore and be subsequently moved out of the pore by the flooding fluid. Remaining oil trapped in a dead end (as shown in Figure 31) the similar characteristics of residual membrane oil and have an identical separating mechanism from pore wall by the binary system. The one divergence is that the former is trapped in concave dead-ends which can't be swept by water. In comparison with water flooding, the polymer-surfactant binary system has a viscosifying influence, and its low IFT can emulsify oil, which increases the viscosity, the improvement of viscosity allows the co-injection fluid to enter the dead end that cannot be submerged by water, and later separate the remaining oil from the pore wall in a similar process as segregating membrane remaining oil. Due to low IFT, the surfactant- polymer flooding system improves oil wash efficiency and displaces remaining oil in column shapes, an isolated island, and membrane, where the viscosifying effect plays an important role in sweeping ability enhancement, mobilize residual oil caught in dead ends a boost oil recovery.

Regarding the recovery factor percentage, the co-injection of polymer-surfactant recorded a less RF value (61%) compared to the polymer-surfactant sequence injection (63%) by 2% .This result may be due to the ability of surfactant first to reduce the IFT value between

the oil and the water, which make it easier after for the oil to be removed by polymer injection (polymer increases the mobility ration).

- In the polymer flooding, the polymer concentration considers one of the critical factors in oil recovery. Considering the economic aspects, the Suitable polymer concentration should be restricted. The average polymer concentration is between 100 to 2,000 ppm, but in this experiment, a low concentration was favored for injection due to the low viscosity of the oil. Tests 1-2 and 2-2 were conducted to quantify the impacts of polymer concentration in the micromodel oil recovery tests. The two solutions were infused within the micromodel with 0.01 ml/hr. as the injection rate. Two different concentrations of 10^{-3} and 3.10^{-3} wt. % were applied. The details and results of the experiments are delivered in

- Table 6. The results proved that increasing of the concentration of polymer caused an improvement in RF by 4%.

- Nine images, as it is shown in Figure 34, presented the residual oil saturation changes as a function of the injected pore volume. In this experiment, an aqueous solution of xanthan gum with 10^{-3} wt. % as concentration was used with a flow rate of 0.01 ml/hr. To create these diagrams (see Figure 33), a discontinuity method where the oil saturation was measured each hour after the injection was stopped than an image was taken. As it is illustrated in Figure 34. The restarting and the stopping of this procedure caused a small pressure kick, but for the simplicity reason, this effect was neglected. Using the previous equation (14), it was able to calculate the recovery factor. Figures 33 and 34 show the oil recovery at several pore volumes injected. Polymer-Surfactant and water flooding show the same variations, where the recovery factor increases with increasing of injected pore volume. The average recovery factor of water flooding experiment is 59%, and it is achieving its maximum only at the end of injection. Also, Figure 33 a) confirms that the recovery factor is increasing in the tertiary flooding corresponded to the secondary case by 30%. The surfactant-polymer (seq) achieve a recovery factor of 70%. This larger oil recovery is resulting of the ability of surfactant decrease the interfacial tension between oil and water and improve microscopic efficiency and the role of polymer in enhancing the mobility ratio.

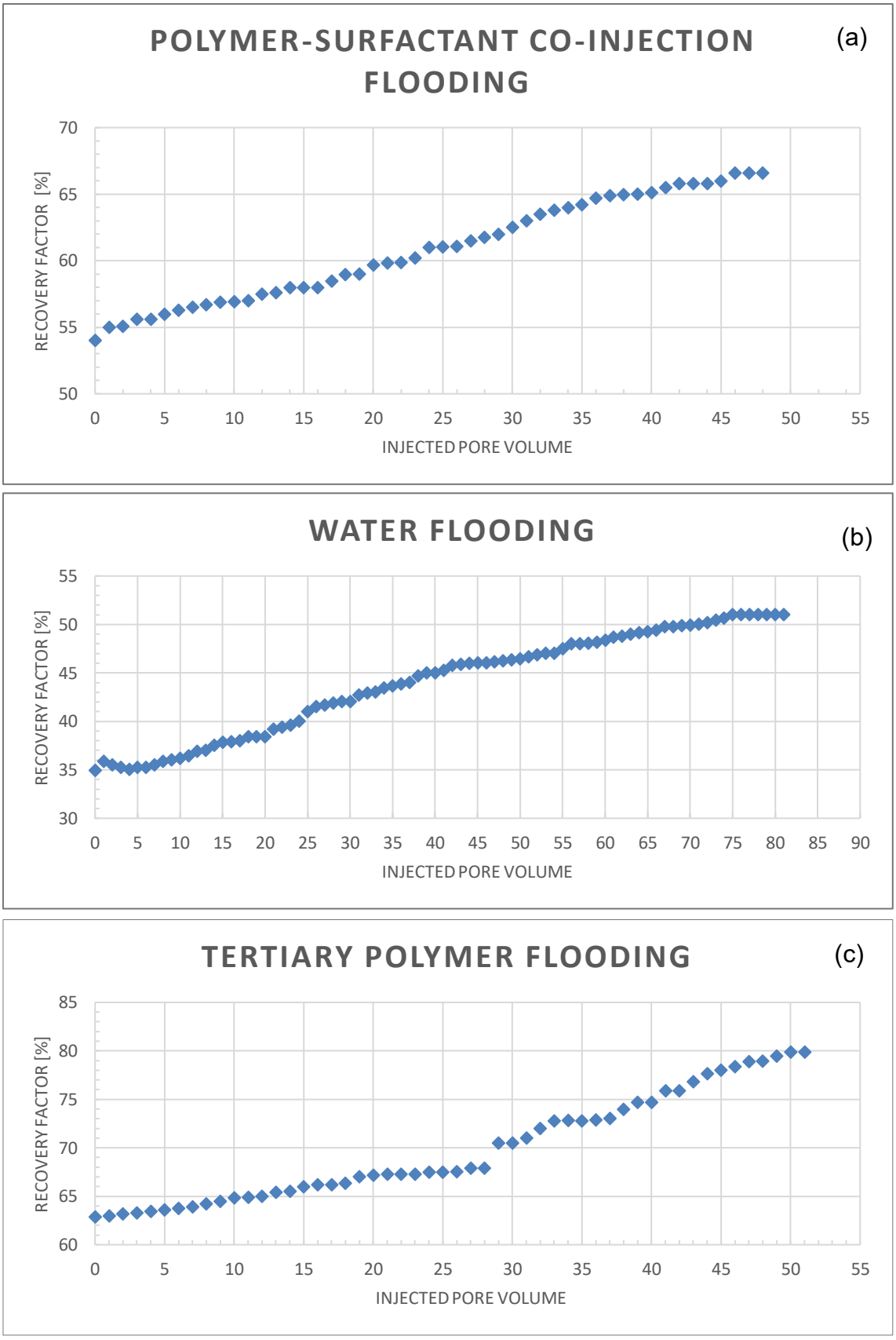

Figure 33: plots show the relation between the injected pore volume and the recovery factor for the different EOR methods.

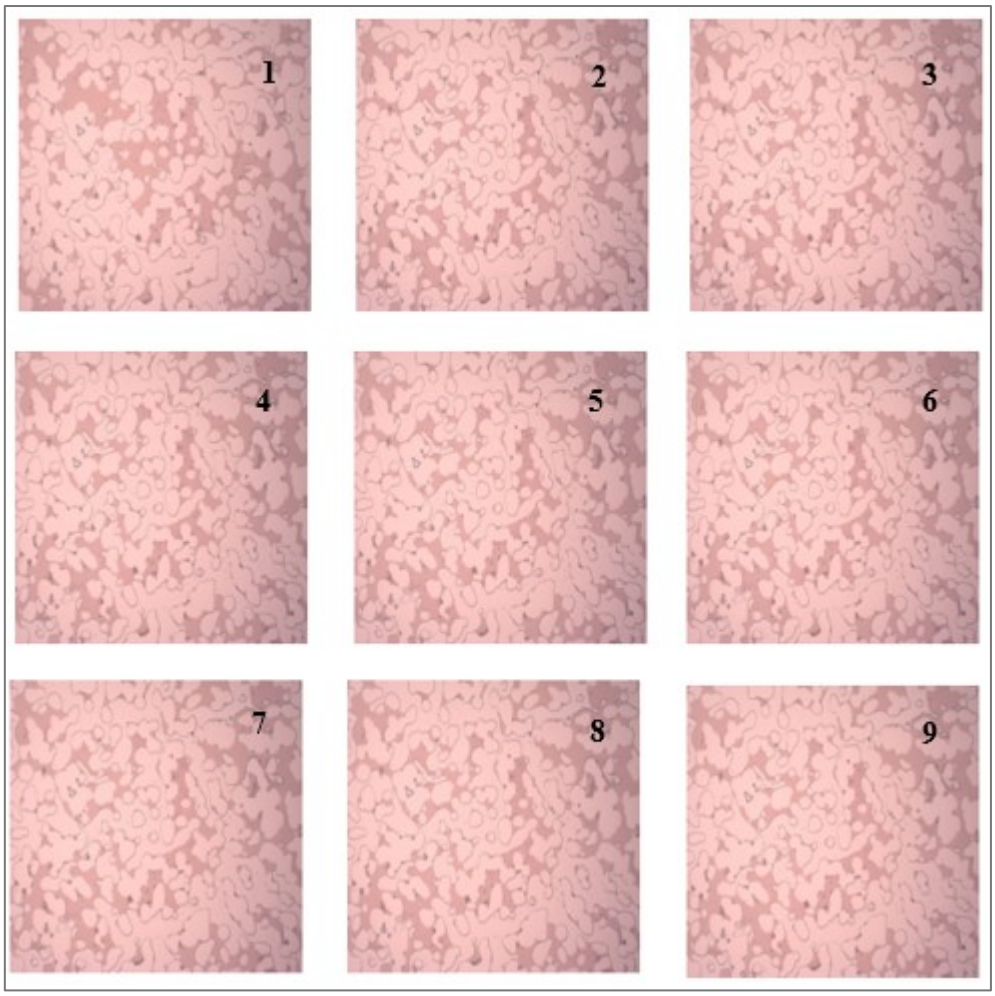

Figure 34 : The images show the oil displacement during the experiment in each one-hour interval.

- Surfactant alternated gas (SAG), is the injection of a surfactant slug followed by a slug of gas. This method is used to generate foam is formed in situ in the porous media. Since 1930s gas injection has been used as an enhanced oil recovery method. Nevertheless, the viscous fingering and the gravity override which is caused by the gas low viscosity and density can effectively reduce the sweep efficiency. These kinds of obstacles can be overcome by using foam to trap the gas and increase the apparent viscosity and diverting the flow to the unsweep zone. The foam structure can change due to three phenomena: first, the film collapses because of capillary pressure, second liquid drainage through the films, which is neglected at the pore scale, and finally coarsening, due to gas diffusion between bubbles. This work focusses on the foam flow behaviour regarding the bubble structure and size distributions, and the relationship between foam quality and its mobility. The foam experiments were conducted by sequential injection of surfactant and gas in micromodel.

The surfactant used for the experiment was Poly (ethylene glycol) (12) tridecyl with 1 wt.% concentration. The surfactant solution was injected using a syringe pump fitted with a 3 mL plastic syringe. A frame of images was taken at specific location to ensure that the foam was well established and to avoid any potential access or end effect. Images of the micromodel, and the foam within the pores, were recorded using a high-resolution video camera connected to the microscope. This camera had a resolution of 2592 * 1944 pixels, where the images were taken in a time-lapse of 20 to 30 s. the foam images were then processed and binarized using the ImageJ software; and then the edges of the bubbles were marked in red colour using MATLAB. The foam images in the micromodel were taken at the beginning of the experiment and at different stages during the gas injection as it is shown in Figure 35 (1-8).The coarse foam is similar to gas slug characterized by relatively huge bubbles dispersed in the liquid as illustrated in Figure 35 (2-3-4) below where the large bubble of air presented in the white colour with red edges. During the experiment, it was observed that the first coarsening happened in the sections along the centre of the porous media, while there was still some current in the walls. This can be detected in a composite made of Figure 35 (2- 3- 4). These images show that in the upper and lower sections of the media, the bubbles coarsened in the first 420 sec. while there are yet few flows in the midsection due to internal pressure gradients in the chip. After 480 seconds, the diffusion of the bubble between each other had resulted in desperation of large number of bubbles and generation of lamella with minimum energy configuration at the last part of the micromodel, where, the first part act as a mixture of dispersed bubbles it can be observed in Figure 35(1). In the pore throats, apart from a few lamellae which maintained stable configurations across pores (see Figure 35 (8)). The progressing of the coarsening showed that not all the bubbles coarsen at one certain time, the sequence of the image presented in Figure 35 gives an overview about bubble evolution during the coarsening process, the time difference between each image is between 30 to 90 seconds. Initially, there were 291 bubbles which characterized by a large surface area in the porous media, this coarsened to 134 bubbles after 150 seconds (Figure 35(1-4)). The time at which approximately the half number of bubbles disappear is called the characteristic time of coarsening, in this case, is around 150 sec. After this characteristic time, 46% of the bubbles remained in the micromodel. The disappearing of large bubbles leads to the creation of many small bubbles; and thus, increase the number of bubbles to 433 at 480 sec (Figure 35(8)). At the same time, a lamella starts to form in the last part of the micromodel.

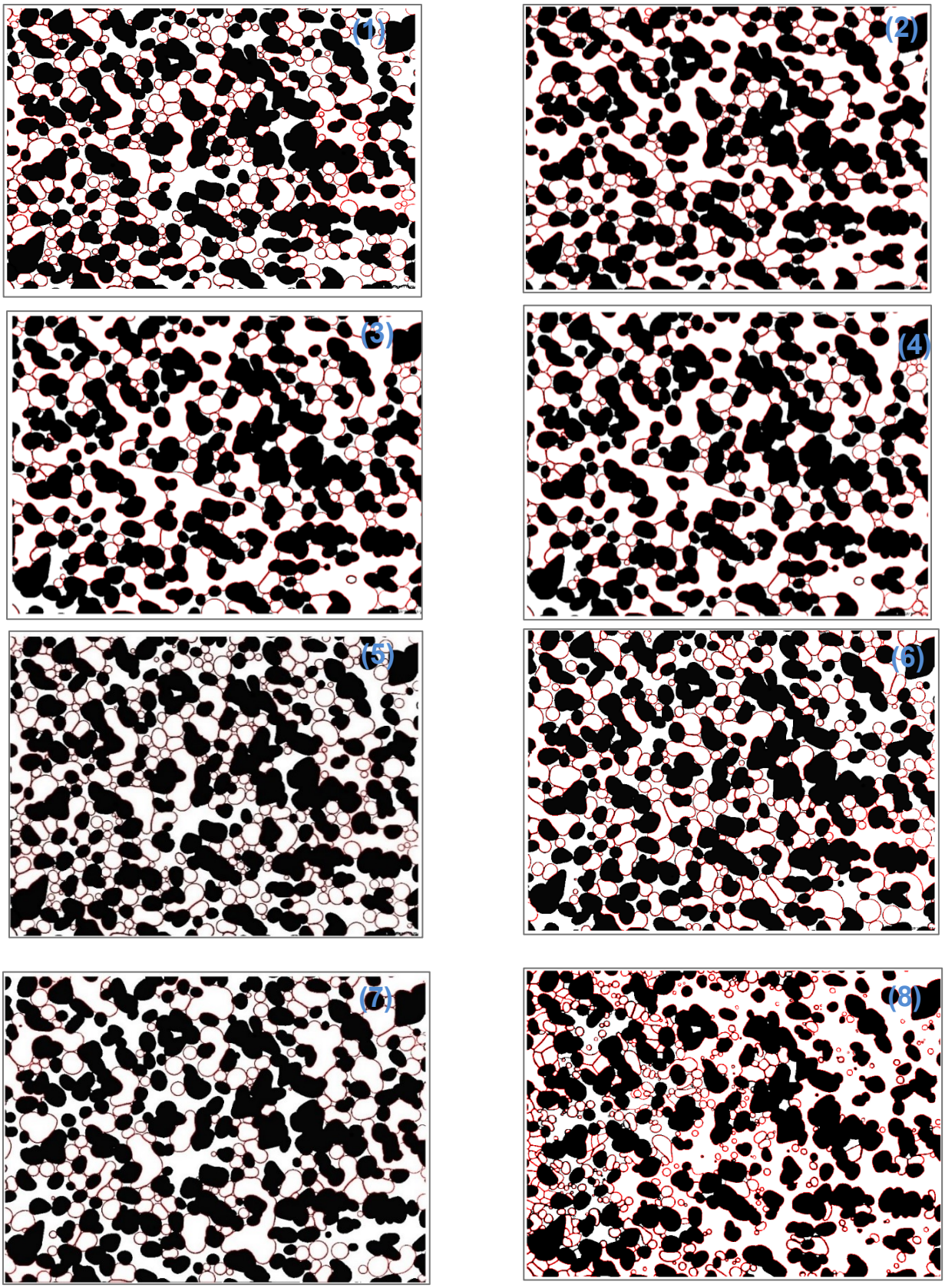

Figure 35:A sequence of images present the bubbles flow during different times:1) 210 s; 2)300 s; 3)330 s; 4)360 s;5) 390s ;6) 420s ;7)450s; 8)480s.

- A bubble size distribution measurement started at T= 210 s, several pictures at the different time were taken to observe the bubble size distribution changes along the experiment. Using these images, four histograms (see Figure 36) were created showing how many bubbles share the same area size. In the first image and histogram at 210 sec can be seen that the foam had a predominance of bubbles size relatively smaller than the pores, where the average bubble area was 300 mm^2. Confirming to last conclusion the second histogram at 360 sec show fewer bubbles number with much smaller size compared with the first one.

  After 90 seconds and due to the gas flow, the bubble size distribution had evolved into a bimodal distribution. First, the beginning to the midway of the micromodel exhibit many small bubbles trapped in the pore throats, secondly the generation of the lamella was observed at the end of the micromodel. Finally, in several literature reviews [6] coarsening is considering a self-similar, meaning that the bubble structures topology persists invariant with time, which confirms the experiment outcomes that shows similar results (after the coarsing the bubbles size remains constant around 100mm^2).

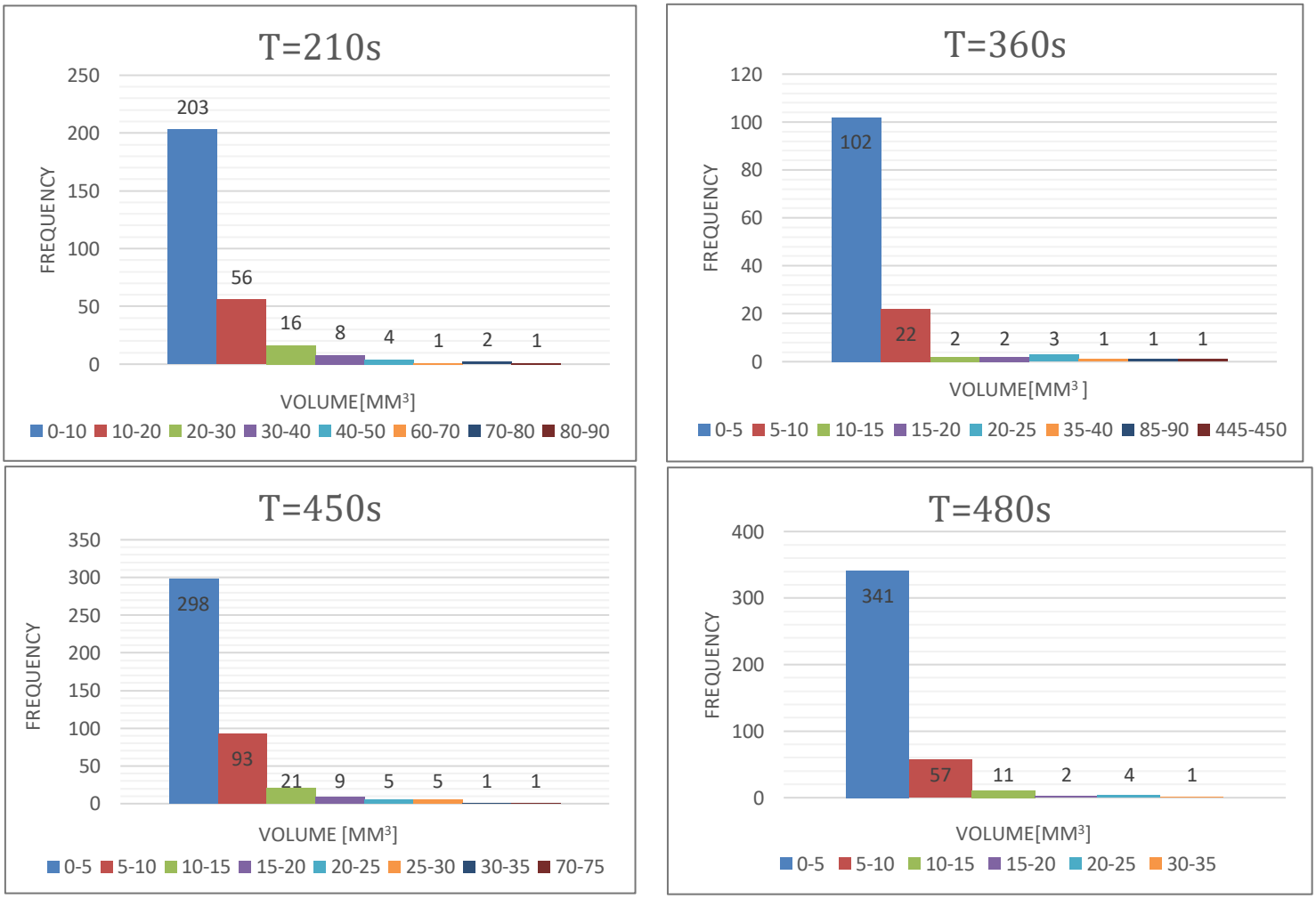

Figure 36: The plot shows the frequency of bubbles sizes corresponding to their volume at different time steps.

Also, the different data (based on data from Figure 37) was plotted in a single graph (see Figure 36), showing different volume versus frequency of bubbles at four-time steps. The Figure 37 present as similar behavior for the different time steps where the smaller bubbles have higher frequency compared to the larger bubbles due to coarsing effect. Conforming to the previous conclusion, that at the beginning and the end (210s and 480s) have larger number of small bubbles then bigger ones, otherwise the middle time (360s and 450s) have a higher number of large bubble volume.

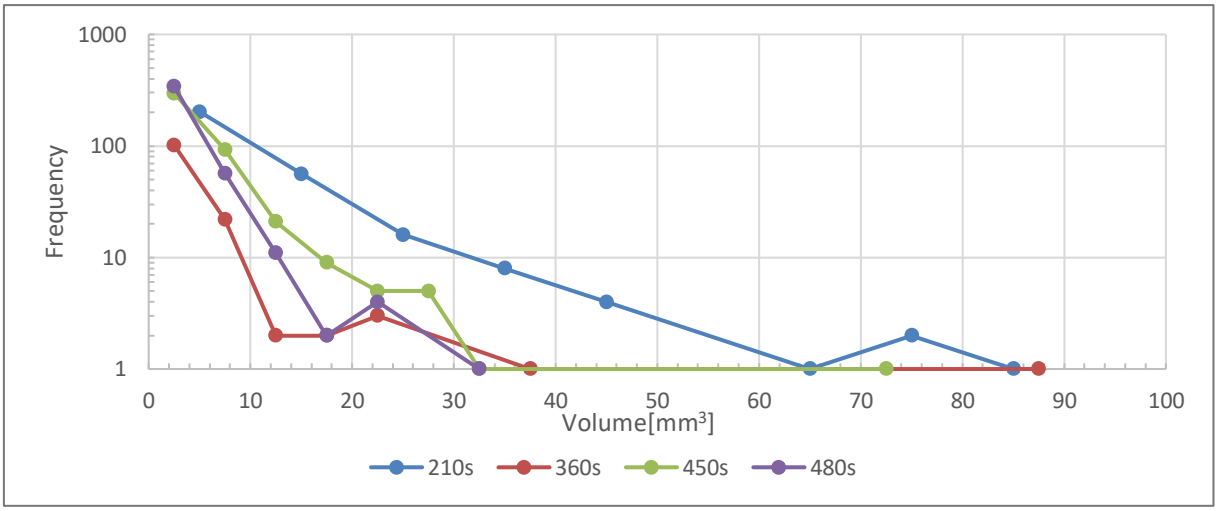

Figure 37: Bubble size distribution at different steps in time

- First before making any conclusion about the size effect on the velocity of the bubble it necessary to take into consideration several issues. For example, due to the limited numbers of bubbles that were an investigation, the statistics data regarding the bubble size versus the velocity were insufficient to conclude an accurate conclusion, where the small range of bubble size doesn't permit to examine the size effect on the bubble behavior. Secondly, it was not possible to assign a field vector because of the large size of the bubble if we compare it with particles. To understand the bubble size effect on the foam mobility a tracking velocity of bubble swam technique was carried out using ImageJ as image by tracking moving objects. The input of this plugin is a sequence of image frames F (x, y, t) where x, y are spatial coordinates. Each frame is captured at fixed time intervals and t represents the frame time in the sequence. First, the x y and z calibration values were set as well as the time interval value based on the used scale in the experiment; the definition of the different area possible manually, so the software look for the expected area range and neglect the unnecessary noise. Then to each selected area velocity vector was assigned.

During bubbles formation, different types of bubbles shapes were observed: touching bubbles (bubble clusters) and irregular bubble shapes. With these characters, it's challenging to recognize and separate the bubbles. Therefore, the efficiency of bubble tracing over a sequence of pictures is decreased. Consequently, five frames with a limited number of bubbles were considered as presented in Figure 38 (intervals of 30ms and 12960*1944 pixels size). The software allows bubble geometric properties to be measured in the image sequence and compiled into a data structure.

- To identify the of bubbles, enhanced image processing process was developed. This process is based on improving the contrast between the background and the bubbles after filling them, then threshold was used to neutralize the effect of dark areas or uneven light distribution. Each frame is converted into a binary image (see Figure 38), where geometric properties are measured. These objects are converted into a data structure containing bubble properties. Table 7 shows the position coordination, area, and the velocity. By using this data, it was possible to create a plot (Figure 39) showing the velocity variation versus the bubble sizes.

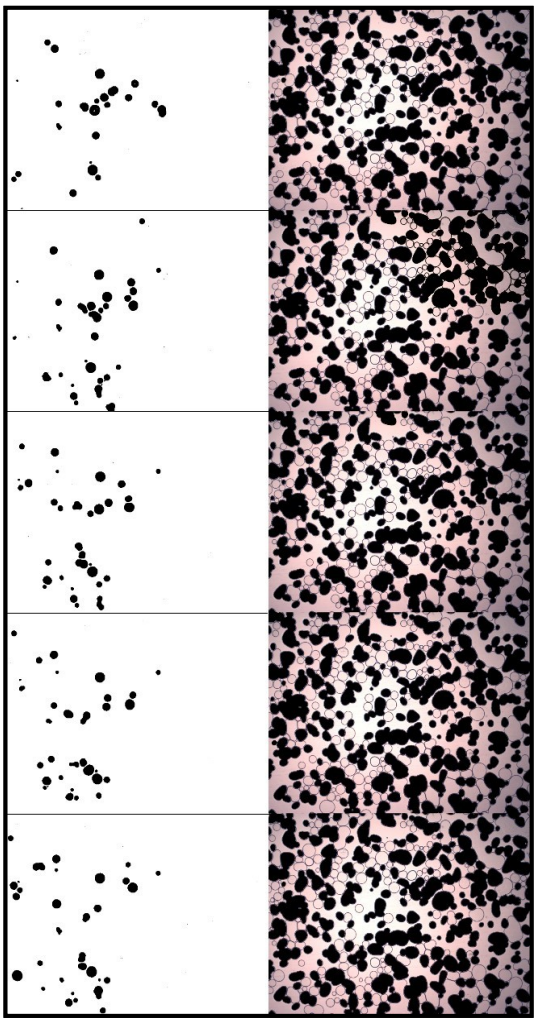

Figure 38: In the left possible matching bubbles (black dots) from 5consecutive images and in the right side shows the grains black.

		X	Y	Distance	Velocity (mm /s)	Area (micron)	Area (mm^2)
1	2	1236	696	38.730	3.228	2,5	2,50E-02
1	3	1132	696	138.320	11.527	2,2	2,20E-02
1	4	464	892	925.894	77.158	2,2	2,20E-02
2	2	992	840	79.087	6.591	4	4,00E-02
2	3	908	948	181.972	15.164	4,1	4,10E-02
2	4	788	992	169.990	14.166	3,8	3,80E-02
2	5	488	872	429.736	35.811	3,2	3,20E-02
4	3	144	332	1614.101	134.508	1,3	1,30E-02
4	4	60	204	203.625	16.969	1,3	1,30E-02
4	5	28	240	64.061	5.338	1,3	1,30E-02
6	2	1244	924	388.324	32.360	3,8	3,80E-02
6	3	1196	924	63.840	5.320	3,9	3,90E-02
6	4	1208	880	60.657	5.055	4	4,00E-02
6	5	1228	712	225.018	18.751	3,9	3,90E-02
8	3	736	1476	417.578	34.798	4,4	4,40E-02
8	4	668	1472	90.596	7.550	4,4	4,40E-02
8	5	112	1584	754.334	62.861	2,5	2,50E-02

Table 7 : The data extracted from the tracking plug showing the position coordination, velocity and area.

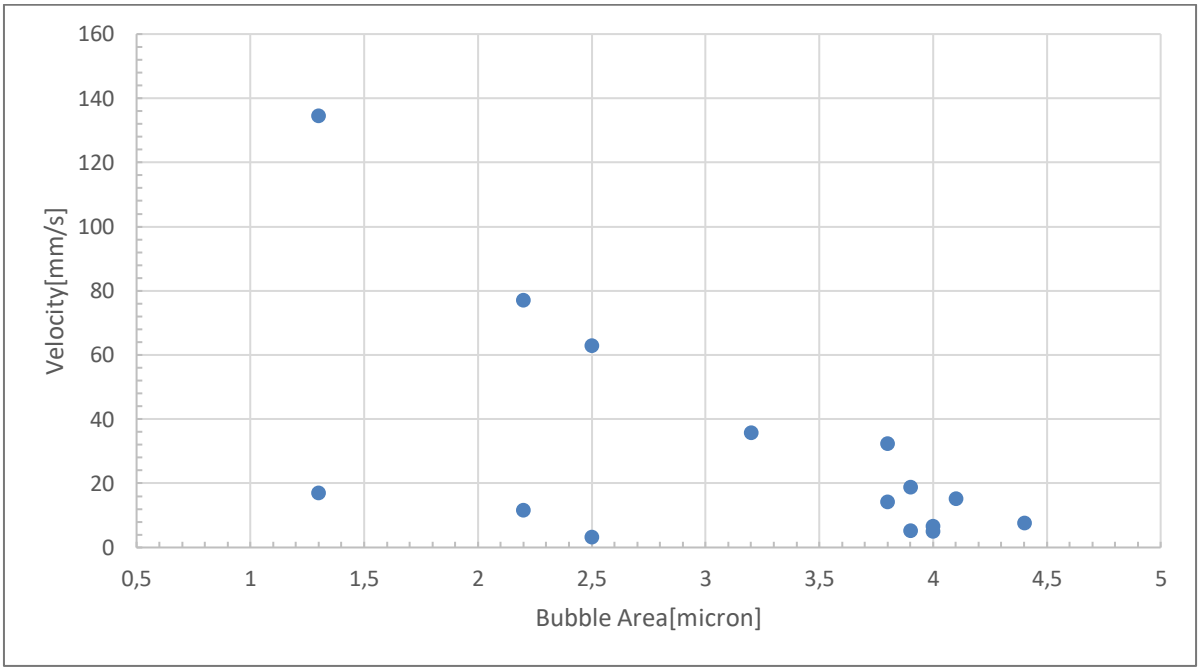

Figure 40: A plot present the bubble sizes versus the velocity

Despite the restrictions of the experiment, it is possible to get a general idea about how the bubble sizes effect to the velocity.

The measurements were converted to plot where this data created 2 main overlapping size ranges 1.3-2.4 and 2.5-4.4 micron but with a huge fluctuation of velocity values cause by that same bubbles size don t follow the same path. Despite these variations, it is still possible to distinguish between two velocity ranges. The first range is related to larger bubble size with much less velocity (3-35 mm/s) with an average of 20mm/s while the second range characterizes the small bubble size with an average velocity of 49 mm/ s, which is twice as much the velocity of the larger bubbles. The results of this experiment show that high-quality foam which consists of large bubbles have a lower mobility than the low-quality foam (smaller bubble size)

- **Future work**

  During the investigation, several issues exited such as defending the straightforward relationship between the bubble sizes and the velocity and indirectly about the effect of different sizes on the foam mobility. First, the limited number of the bubble due to technical consideration (for example having restricted images with the same representative element area and knowing interval time and also uneven lighting), the size range was small also, the high fluctuation of velocity values makes it hard to extract a clear trend to describe the effect of size on the bubble velocity. Because of these issues, the collected statistics data were insufficient to make a relatively accurate conclusion.

  For further investigation, it is possible to study the effect of surfactant type on the foam topology which affects its velocity, as well as testing different gas flow rates. Likewise examining the foam mobility in terms of bubble interactions, in both ways small to large and large to small bubble size.

8.1 Issues

A lot of challenges occurred before during and even after an experiment. Challenges and failures do not only cause only difficulties, but they also help to improve and show weaknesses in the aperture and workflow of tests. Accidents and human failure usually set back the work for a few days. Some of these problems and accidents are detailed in the following to give a better knowledge of experimental condition. Issues are posted in the chronological orders of innovative workflow.

- **Polymer mixing and filtering**

Usually, the polymer blending is insufficient, and small undissolved polymer particles are observed. These undissolved particles can result in pore throats plugging. The mixing procedure is done at slightly elevated temperatures of 30°C, but in this work, it wasn't possible to elevate the temperature due to equipment limitation. Sometimes even the elevated temperature is not sufficient to guarantee smooth operation, and therefore all polymer solutions are filtered. To filter the solution, a cartridge filter with average filter particle size of 15 µm was used.

- **Broken and leaking tubing**

When broken or leaking tubing is noticed early enough, it is possible to change them by new ones, and the experiment is carried out. But leaking or broken pipe during a flood cannot be adjusted or renewed fast enough in order not to falsify the experimental outcome. Leaking tubing can be recognized by abnormal pump pressures or rates during the experiment. Also, small drops on the surface of the desk can be a sign of leaking tubing. Before starting any experiment, cleaning the desk is an essential part

- **Air in tubing**

Air bubbles in the tubing lead to incorrect measurements and results. When attaching and detaching the pump to the fluids vessel, small pockets of air are trapped in the connection and move into the container when pumping is started. Trapped air induces wrong permeability measurements which in consequence cause a false assumption that the micromodel is not usable for the experiment. The difficulty is solved by connecting the second valve to the fluids vessel, where the air is discharge when pumping starts.

- **Connect tubing to micromodel**

The connection from the oil vessel to the micromodel inlet port has to be tightened very slowly. If tightened too fast, a high volume of oil is pushed into the micromodel in a short time and result in very high pressure. If the pressure passes a particular limit, the micromodel will break. Hence the connection is screwed very slowly, and very low pressure is used to make the connection.

➢ Image Analyses

Uneven illumination of the pictures makes them very difficult to be analyzed. To diminish the impact of lighting, only the middle section of the images is cut out and used for further processing. Results of recovery and swept area are required to judge the experimental success. A significant disadvantage of the micromodel is the missing possibility to perform any material balance.

Inlet ports and O-ring cravings occupy ten times greater volume than the micromodel matrix. This large dead volume is a severe problem in measuring the amount of the displacing or displaced phases. Additionally, the volume of liquid used for a whole experiment is so small that it does not reach the outlet port of the outlet fracture and then it cannot even be assembled for measurement. Several other attempts to reach a material balance with weighting and using finer injection ports were not successful. So, consequently, the high-resolution photographs of the pore structure in the micromodel are taken to determine irreducible water saturation (S_{wi}), water saturation at breakthrough (S_{btp}) and remain oil saturation (S_{or}).

The whole area of the micromodel should be captured; this is why the micromodel is subdivided into three equally sized rectangles using pendent drop camera. These moments are first after oil saturation to determine S_{wi}, secondly after the breakthrough of the polymer solution at the outlet fraction to determine the Sbtp, and finally, after 48 hours which refers to 50 swept pore volumes of the micromodel to determine S_{or}.

9 Conclusion

This work describes the experiments associated to the EOR techniques such as polymer flooding, surfactant, surfactant-polymer, and foam using the university laboratory. Different tests were created and performed to examine the impact of the previous solutions in the decrease of the residual oil saturation.

The baseline for all later experiments was the water flood done at the very beginning of the study. As expected, water flooding resulted in the lowest recovery factor because of the high IFT between the water and the oil. Due to the surfactant ability to reduce the IFT and polymer in increasing the sweep efficiency, the highest recoveries were obtained with surfactant and surfactant-polymer flooding where the average recovery factor reached 61 %. In the analysed images oil threads and elongated clusters were observed that might be relevant to low interfacial tension because of in-situ soap generation.

A foam generation experiment was performed base on the SAG technique; which is first a surfactant injection then followed by gas slug. This method generated two types of foam quality (weak and strong). This experiment showed that the coarsening of the bubbles doesn't happen at the same time. In addition the relationship between the bubble sizes and the velocity was investigated; the result show that the smaller bubbles have a higher velocity compared to the larger ones. As indirect conclusion good foam quality characterises by low mobility.

In the end, the main scope of this thesis is more concerning educational reasons to create and optimize the experiments setting in the university laboratory for better results for different EOR techniques and to develop a protocol which describes and explains the physics behind these mechanisms to help future students.

The influence of many other parameters on the different flooding processes such as the type of the solution, concentration, salinity, brine composition and temperature can be investigated. Furthermore, the fluid topology, the capillary desaturation analysis regarding the microscopic and macroscopic capillary numbers can also be investigated as future work. Additional examination and focusing on specific mechanisms, particular porous media patterns can be created and manufactured. Finally, concerning the foam, more experiments could be done to investigate the influence of surfactant type and its concentration on foam quality and mobility, as well as different flow rate and pressure.

10 References.

[1] S. Pwaga, C. Iluore, Ø. Hundseth, F. J. Perales and M. U. Idrees, "Comparative Study of Different EOR Methods," Norwegian University of Science & Technology, Trondheim, Norway, Trondheim, Norway, 2010.

[2] R. Hilfer, Transport and Relaxation Phenomena in Porous Media, 63, 14 March 2007.

[3] Leal and L. Gary, Advanced Transport Phenomena: Fluid Mechanics and Convective Transport Processes, Cambridge University Press, June 2012.

[4] R. T. Armstrong, A. Georgiadis, H. Ott, D. Klemin and S. Berg, "Critical capillary number: Desaturation studied with fast X-ray computed microtomography," 9 January 2014.

[5] J. J.Sheng, "Status of surfactant EOR technology," *Science direct,* pp. 97-105, June 2015.

[6] N. Getrouw, "The Static and Dynamic Behaviour of Foam in a Model Porous Media," the Delft University of Technology, September 9, 2016.

[7] M. Buchgraber, "An Enhanced Oil Recovery Micromodel Study with Associative and," University of Leoben, Austria, 2008.

[8] C. J. J. Chatenever A, "Visual examinations of fluid behavior in porous media-part 1," vol. 4, no. 06, p. 4(6):149–156, 1953.

[9] R. L. Chuoke, P. v. Meurs and C. v. d. Poel, "The instability of slow immiscible, viscous liquid-liquid displacements in permeable media," 1959, p. Petrol Trans AIME 216:188–194.

[1] Thompson, TanyaE and JewellKevin, "Ringfield lithography". Nokia Bell Labs AT&T Corp Patent US5315629A, 10 10 1990.

[1] C. W. Hull, "Apparatus for production of three-dimensional objects by stereolithography". Patent US4575330A, 08 08 1984.

[12] C. Iliescu, B. Chen and J. Miao, "On the wet etching of Pyrex glass," *sciencedirect,* p. A 143 (2008) 154–161, 2006.

[13] *World Precision Instruments,* 2017.

[14] W. Bierwerth, Tabellenbuch Chemietechnik, V. G. &. C. K. Nourney, Ed., Haan-Gruiten: Verlag Europa-Lehrmittel, 2005.

[15] T. J. Mason and J. P. Lorimer, Applied Sonochemistry, Weinheim: Wiley-VCH, 2002.

[16] Edwin C. Moritz and Natalie Barron, "Wattenberg Field Unconventional Reservoir Case Study," in *SPE Middel East Unconventional Gas Conference*, Abu Dhabi, 2012.

[17] S. Kenzhekhanov, "CHEMICAL EOR PROCESS VISUALIZATION USING NOA81 MICROMODELS," Colorado School of Mines, Colorado.

[18] Mostafa Borji, "Alkali-based Displacement Processes in Microfluidic Experiments: Application to the Matzen Oil Field," 2017.

[19] A. Firoozabadi and N. Rezaei, "Macro- and Microscale Waterflooding Performances of Crudes which form w/o Emulsions upon Mixing with Brines," *energy and fuels,* p. 12, January 27, 2014.

[20] T. Ransohoff and C. Radke, "Mechanisms of Foam Generation in Glass-Bead Packs," vol. 3, no. 02, May 1988.

[21] T. O. Allen and A. P. Roberts, Production Operations, Well Completion, Workover, and Stimulation Volume 2, Tulsa, Oklahoma: OGCI,Inc.,PetroSkills,LLC., 2008.

[22] M. Lacey, C. Hollis, M. Oostrom and N. Shokri, "Effects of Pore and Grain Size on Water and Polymer Flooding in Micromodels," *energy and fuels,* p. pp 9026–9034, 2017.

[23] N. Karadimitriou and S. Hassanizadeh, "A Review of Micromodels and Their Use in Two-Phase Flow Studies," *Vadose Zone Journal,* August 2012.

[24] P. Abgrall and A-MGue, "Lab-on-chip technologies: making a microfluidic network and coupling it into a complete," *IOPSCIENCE,* vol. R15–R49, 2007.

[25] S. Thomas and S. Ali, "Micellar Flooding and ASP – Chemical Methods," University of Alberta, 1999.

[26] Polczer and Shaun, “Petroleum Economist,” 15 02 2012. [Online]. Available: http://www.petroleum-economist.com/Article/2979412/News-Analysis-Unconventional/Mind-the-oil-sands-price-gap.html. [Accessed 20 02 2012].

[27] "SIGMA ALDRICH," 2017. [Online]. Available: http://www.sigmaaldrich.com/catalog/product/sigma/g1253?lang=de&region=AT.

[28] A. MHowe, A. Clarke, J. Mitchell and J. Hawkes, "Visualising Surfactant EOR in Core Plugs and Micromodels," SPE, 2015.

[29] B. Das, S. Gogoi and D. Mechc, "Micellar-polymer for enhanced oil recovery for Upper Assam Basin," *SciznceDirect,* vol. 3, no. 1, 1 March 2017.

[30] UngerMA, ChouHP, ThorsenT, SchererA and S. Quake, Monolithic microfabricated valves and pumps by multilayer soft lithography, Department of Applied Physics, California Institute of Technology, Pasadena,, 2000, p. Science 288(5463):113–116.

[31] WeidongLIU, LitaoLUO, G. LIAO, LuoZUO, YunyunWEI and W. JIANG, Experimental study on the mechanism of enhancing oil recovery by polymer - surfactant binary flooding, PETROLEUM EXPLORATION AND DEVELOPMENT, August 2017.

[32] Leung and JulianaYukWing, "Accounting for Heterogeneity in Scale-Up of Apparent Polymer Viscosity for Field Scale Application," Society of Petroleum Engineers, 2010.

[33] OmolbaninSeiedi, M. Rahbar†, MoeinNabipour, MohammadA, Emadi, M. H, Ghatee‖ and S. Ayatollahi, "Atomic Force Microscopy (AFM) Investigation on the Surfactant Wettability Alteration Mechanism of Aged Mica Mineral Surfaces," *Energy & Fuels,* vol. 25 (1), p. pp 183–188, 2011.